frontiers | Frontiers in Earth Science

TYPE Original Research
PUBLISHED 06 March 2025
DOI 10.3389/feart.2025.1523033

OPEN ACCESS

EDITED BY
Hu Li,
Sichuan University of Science and Engineering, China

REVIEWED BY
Eun Young Lee,
University of Vienna, Austria
Long Luo,
Chongqing University of Science and Technology, China

*CORRESPONDENCE
Siyi Fu,
fusiyi@cdut.edu.cn

RECEIVED 05 November 2024
ACCEPTED 31 January 2025
PUBLISHED 06 March 2025

CITATION
Zou C, Fu S, Hu J, Hou L, Chen A, Xia Y, Liu H, Yu Y and Chen H (2025) Geological characteristics and controlling factors of deep tight gas sandstone reservoirs in the Upper Paleozoic of the western Ordos Basin, northwest China.
Front. Earth Sci. 13:1523033.
doi: 10.3389/feart.2025.1523033

Geological characteristics and controlling factors of deep tight gas sandstone reservoirs in the Upper Paleozoic of the western Ordos Basin, northwest China

Chengyu Zou[1,2], Siyi Fu[1,2,3,4]*, Jianling Hu[5,6], Linjun Hou[7], Anqing Chen[1,2,3], Yuqing Xia[8], Hao Liu[1,2], Yu Yu[1] and Hongde Chen[1,2,3]

[1]State Key Laboratory of Oil and Gas Reservoir Geology and Exploitation (Chengdu University of Technology), Chengdu, China, [2]Institute of Sedimentary Geology, Chengdu University of Technology, Chengdu, China, [3]Key Laboratory of Deep-time Geography and Environment Reconstruction and Applications of Ministry of Natural Resource, Chengdu University of Technology, Chengdu, China, [4]College of Petroleum Engineering in China University of Petroleum (Beijing), Beijing, China, [5]Exploration and Development Research Institute of PetroChina Changqing Oilfield Company, Xi'an, China, [6]National Engineering Laboratory for Exploration and Development of Low-Permeability Oil and Gas Fields, Xi'an, China, [7]Wuxi Research Institute of Petroleum Geology, SINOPEC Petroleum Exploration and Production Research Institute, Wuxi, China, [8]Exploration and Development Research Institute, SINOPEC Jianghan Oilfield Company, Wuhan, China

Recent exploration has confirmed industrial gas flows from several wells in the western Ordos Basin, suggesting considerable hydrocarbon exploration potential. However, prior research on characteristics of tight sandstone reservoirs, diagenetic evolution, and controlling factors in the Upper Paleozoic of western Ordos Basin remains limited. Here, underpinned by extensive cast thin-section identification and integrated with field emission scanning electron microscopy, nuclear magnetic resonance, and mercury intrusion porosimetry, we investigated the characteristics of tight sandstone reservoirs in the western part of the Upper Paleozoic strata of the Ordos Basin and examined the impact of various factors on the formation of high-quality reservoirs. There are differences in sandstone composition and type, and reservoir properties among different formations of the Upper Paleozoic of western Ordos Basin. The main pore types in the Carboniferous Yanghugou Formation and the Permian Taiyuan Formation were intergranular pores and dissolution pores of lithic fragments, whereas in the Permian Shanxi Formation and He 8, the main pore types were intercrystalline pores of clay minerals and dissolution pores of lithic fragments. In terms of physical properties, the reservoirs of the Upper Paleozoic in the western Ordos Basin have low porosity and low permeability. However, the Permian Taiyuan Formation and He 8 demonstrate better pore-throat connectivity than other stratigraphic levels. The formation of high-quality reservoirs in the Upper Paleozoic of the western Ordos Basin is governed by multiple factors. The Permian Shihezi and Shanxi formations within the alluvial plain facies, Taiyuan Formation barrier bar facies, and Yanghugou Formation delta front facies exhibited the best physical properties. Variations in the original parent rock led to different types of reservoir rock fragments, with a higher content of porosity-enhancing rock fragments correlating to stronger dissolution effects.

Diagenetic processes influence reservoir preservation and development, with rapid burial and compaction being the main causes of densification in the Yanghugou Formation. Cementation impacts reservoir interactions differently over time. Fracture systems in the study area play a key role in improving reservoir permeability. This study offers a scientific foundation for energy-efficient exploration of low-permeability craton basins and new insights for predicting unconventional resources in global marine-to-continental sedimentary systems.

KEYWORDS

tight Sandstone, reservoir Characteristics, controlling factors, western Ordos Basin, Upper Paleozoic

1 Introduction

Although the porosity of tight sandstone reservoirs is generally less than 10%, and the matrix permeability under overburden pressure is less than 1×10^{-3} μm^2 (Sun et al., 2017; Zou, 2014), they have considerable exploration and development potential. Discoveries have been made in the Irish Sea Basin, Colorado's Picea Basin, Western Australia's Perth Basin, and the sedimentary basins of Canada (Kadkhodaie-Ilkhchi et al., 2014; Oluwadebi et al., 2018; Pujol et al., 2018; Stroker et al., 2013). Over the last 2 decades, the exploration and development of China's tight sandstone gas have seen rapid growth, with key findings in the Ordos and Sichuan Basins. They account for approximately one-third of China's natural gas reserves (Yang and Zou, 2022; Zou et al., 2019). Given the great depth and complex diagenesis of these reserves and the associated exploration challenges, it is particularly important to analyze reservoir characteristics, mechanisms of quality reservoir densification, and the interplay of various controlling factors (Karim et al., 2010; Liu et al., 2022; Taylor et al., 2010; Yang et al., 2016).

The Ordos Basin is China's largest oil- and gas-bearing basin, with multiple large gas fields exceeding 1×10^{12}m^3 discovered in Paleozoic strata (Dai et al., 2012; Hu et al., 2020), concentrated in the eastern and northern regions (Figure 1). However, few advancements have been made in the western basin. During the Late Carboniferous, the eastern and western marine areas of the Ordos Basin were interconnected, leading to a unified and similar depositional environment (Yang et al., 2004). Recent exploration results have also confirmed industrial gas flows from several wells in the western basin, suggesting considerable hydrocarbon exploration potential (Wu et al., 2020). However, to date, prior research on the Upper Paleozoic in the western Ordos Basin has predominantly focused on the structural evolution (Wang et al., 2016), provenance (Lv et al., 2017), source rocks (Zhang et al., 2018), and depositional environments (Zhao and Ji, 2005), with limited attention paid to the characteristics of tight sandstone reservoirs, diagenetic evolution, and controlling factors. Thick sandstone deposits in the study area are also viable subjects for investigating tight sandstone-related issues.

The present study investigated the petrological characteristics, physical properties, pore types, and diagenetic processes of the Upper Paleozoic tight sandstones in the Ordos Basin based on extensive cast thin-section identifications, and scanning electron microscopy, nuclear magnetic resonance, and mercury intrusion porosimetry tests. Their diagenetic evolutionary history has been reconstructed, and the impacts of potential controlling factors on reservoir quality have been examined. This study aimed to deepen our understanding of the mechanisms behind the formation of tight sandstone reservoirs and elucidate the key factors controlling the development of tight reservoirs, thereby guiding oil and gas exploration and development and providing case studies for similar research.

2 Geological setting

Located in western China, the Ordos Basin covers an area of approximately 250,000 km^2. It is a cratonic basin characterized by stable subsidence and multiple sedimentary cycles formed on an Archean–Proterozoic basement (Figure 1A). The primary structure of the Ordos Basin is a large, gentle westward-tilting slope divided into six major tectonic units: the Yimeng Uplift, Weibei Uplift, Western Margin Fault Zone, Shaanbei Slope, Tianhuan Depression, and Jinxi Fold Belt (Yang H. et al., 2004) (Figure 1B). The study area is situated over two first-order tectonic units, the Tianhuan Depression and the Western Margin Thrust Belt, comprising several large faults with a thrust–nappe structural system (Figure 1C). Following the Paleoproterozoic era, the pre-Cambrian crystalline metamorphic basement surrounding the Ordos Basin underwent erosion and uplift, leading to the formation of the Alxa and Yinshan ancient lands to the north of the basin and the Qilian–North Qinling ancient land to the south. In the Late Paleozoic, the Alxa and Qilian blocks experienced multiple phases of rifting and volcanic eruptions (Geng et al., 2007; Zhang et al., 2017). They are closely related to the widespread volcaniclastic materials in the western region of the Ordos Basin.

As a result of the Caledonian orogeny during the Early Paleozoic, intense and widespread uplift and erosion of the North China block led to the loss of Middle to Upper Ordovician to Lower Carboniferous strata across most of the Ordos Basin. This process created a substantial north–south oriented paleo-uplift in the central basin, dividing it into eastern and western parts. At the end of the Carboniferous, a rise in sea level connected the eastern and western marine areas, resulting in the formation of a unified basin (Bao et al., 2022; Yang et al., 2004). The Upper Paleozoic strata developed in the western part of the Ordos Basin consist of the Upper

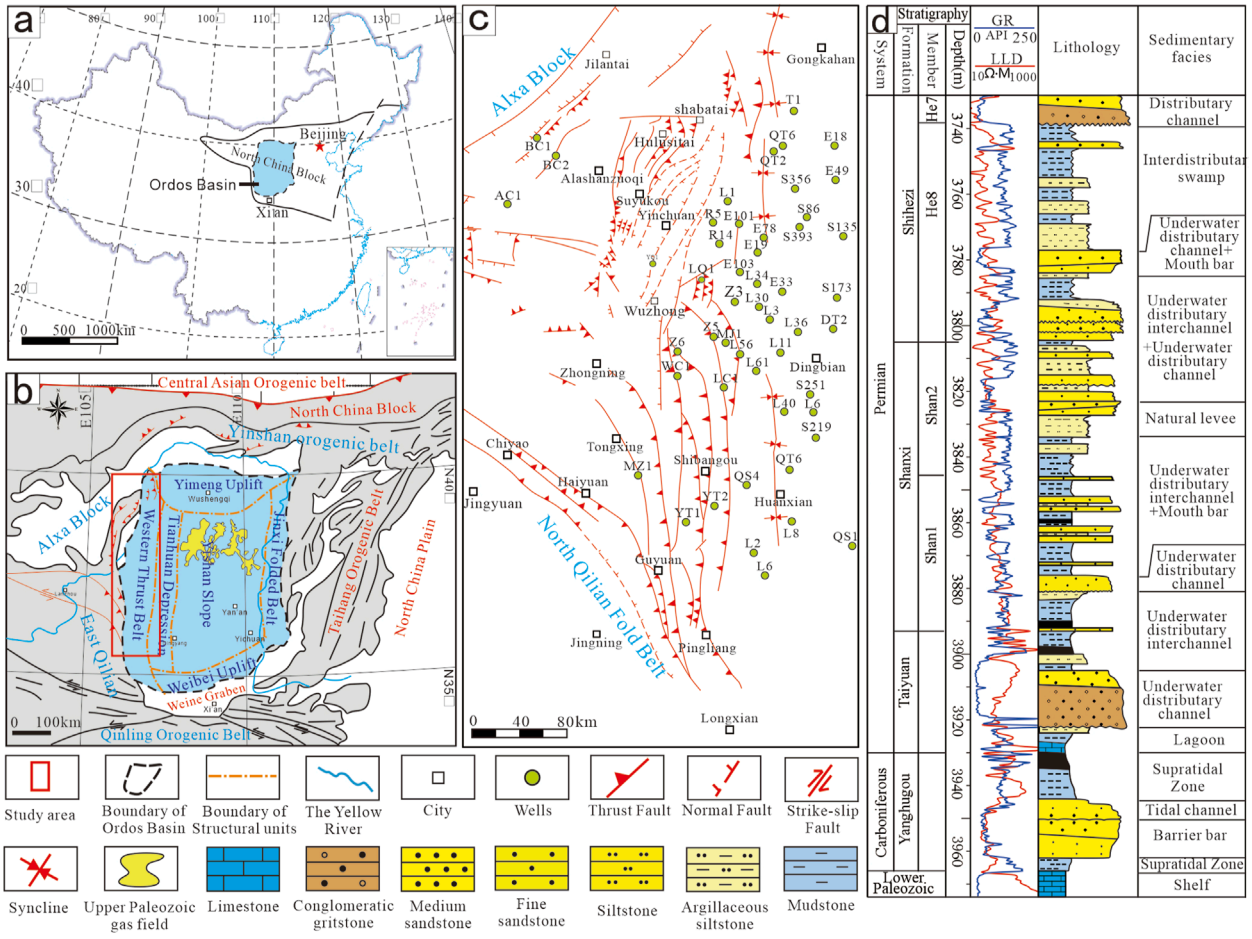

FIGURE 1
Regional structural units and location of the study area. **(a)** Location of the Ordos Basin in China (Darby and Ritts, 2002). **(b)** Tectonic division of the Ordos Basin and the location of the study area (Xiao et al., 2019). **(c)** The location of 50 Wells used in the study. **(d)** Stratigraphic column of the Upper Paleozoic (Well E33).

Carboniferous Yanghugou Formation, Lower Permian Taiyuan Formation, Shanxi Formation, Middle Permian Shihezi Formation, and Upper Permian Shiqianfeng Formation (Figure 1D). Existing exploration and development practices in the gas fields of the Ordos Basin have indicated that tight sandstone gas reservoirs are primarily distributed within the Yanghugou Formation, Taiyuan Formation, Shanxi Formation, and the He 8 member (Yang et al., 2012). Consequently, other minor layers of the Shihezi and Shiqianfeng Formations are beyond the scope of this study.

The western region of the Ordos Basin experienced a sedimentary transition from marine to marine–terrestrial transitional to terrestrial facies during the Early Paleozoic. The Yanghugou Formation consists of clastic coastal sedimentary systems, the Taiyuan Formation of marine–terrestrial transitional delta systems, the Shanxi Formation of meandering river delta–beach bar–coal swamp–littoral shallow lake systems, and the Lower Shihezi Formation of the braided river–braided delta systems, along with lacustrine sedimentary systems (Figure 1D). The Yanghugou and Taiyuan Formations were deposited against a stable cratonic structural backdrop, characterized by early marine transgression and substantial sediment thickness. The lower part of the coal-bearing strata consists of shale interbedded with multiple sets of sandstone (Shen et al., 2022). Meanwhile, the upper part is dominated by mudstone and limestone, with thin coal seams serving as high-quality hydrocarbon source rocks in the west. With a cumulative thickness greater than 200 m and organic carbon content (TOC) in carbonaceous mudstone reaching 25.4%, the liquid hydrocarbon generation stage was completed, making it a potential source for Upper Paleozoic gas reservoirs (Li and Li, 2008). By the Shanxi Period, seawater had receded substantially from the western area, turning it into a nearshore terrestrial sedimentary basin. The northern Yin Mountains and Alxa orogenic belt were gradually uplifted, expanding the land area and providing abundant clastic material for sediment infill. This laid the foundation for continuous river delta development. During the He 8 period, with continuous southward subduction and pushing of the Siberian Plate from the northwest, the northern edge of the North China platform was further uplifted, the stratigraphic datum plane subsided significantly, and the paleoclimate became semi-arid. The alluvial system extensively prograded into the basin and river development reached its peak, marking the main construction period of the sandy reservoirs in the Late Paleozoic (Zhu et al., 2022).

3 Data and methods

Logging data were collected from 50 wells in the western Ordos Basin. PetroChina Changqing Oilfield Company conducted the 50 wells. They were part of the Research Project of PetroChina Changqing Oilfield Company (No. CQYT-CQKTY-2021-JS-2728, 2020-62503). The wells were drilled between 2000 and 2023. The wells are between 65 and 5,000 m deep. Sand body development characteristics were identified through the analysis of lithology, sedimentary structures, and logging data. The analyzed samples were obtained from the core of the Yanghugou Formation to the He 8 member sandstones in the western region of the Ordos Basin. Rock samples of tight sandstone were collected from 53 wells for testing and analysis. A total of 986 nuclear magnetic resonance data points were obtained, including 35 from the Yanghugou Formation, 158 from the Taiyuan Formation, 118 from the Shanxi Formation, and 675 from the He 8 member.

We prepared 200 standard thickness (30 μm) blue epoxy resin-impregnated thin sections to analyze petrological characteristics such as rock framework, cementation features, and pore types. Thin-section examinations and scanning electron microscopy were conducted at the State Key Laboratory of Geological Reservoirs and Development Engineering at Chengdu University of Technology, China. Using a Zeiss microscope (Axioskop 40 Pol) under transmitted light, both plane-polarized and cross-polarized, at least 300 points per thin section were counted to examine the detrital components, matrix, cement, and porosity. To determine the types and characteristics of clay minerals and micropores in the reservoir, 35 samples were cut into small cubes, coated with gold (Au), mounted on aluminum stubs, and observed using a scanning electron microscope (Hitachi S-3000 N, maximum resolution: 3.5 nm). This was conducted at an operating voltage of 25 kV, with magnifications ranging from ×200 to 8,000× to observe the development of target minerals and micropores and acquire high-resolution images of diagenetic minerals. Following the requirements of GB/T 29,172-2012, porosity and horizontal permeability tests were conducted on 1,500 core samples using a Low Permeability Gas Measurement 700 apparatus from Sanchez Technologies at the State Key Laboratory of Chengdu University of Technology. For pore structure analysis, high-pressure mercury intrusion data were collected for 85 samples using a Quantachrome Poremaster-60 mercury porosimeter at the State Key Laboratory of Chengdu University of Technology. Parameters such as capillary pressure curves, threshold pressure, maximum pore radius, median pore-throat radius, and maximum mercury saturation were also collected.

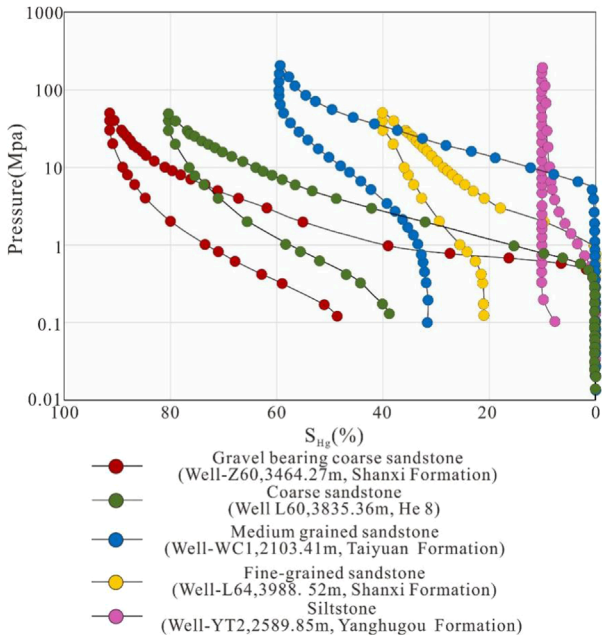

FIGURE 2
Typical capillary pressure curves for HPMI in the tight reservoirs of the Upper Paleozoic in the western.

Additional rock identification data were collected from the PetroChina Changqing Oilfield, comprising 1,062 thin-section samples, along with porosity and permeability data for 378 core samples. This was supplemented with 959 nuclear magnetic resonance (NMR) tests and image logging test data from 50 wells for detailed reservoir analysis. Adhering to the GB/T29171-2012 standard, the National Engineering Laboratory for Exploration and Development of Low Permeability Oil and Gas Fields at the Changqing Oilfield conducted helium porosity and nitrogen permeability experiments on 25 × 25 mm core samples using an ULTRAPORE-200A porosimeter and an ULTRA-PER-MTM200 permeameter. Mercury intrusion tests were performed using a 9,520 model mercury porosimeter to collect high-pressure mercury intrusion (HPMI) data for the 35 × 25 mm samples. The HPMI experiment tested 85 samples comprising 18 from the Yanghugou Formation, 13 from the Taiyuan Formation, 24 from the Shanxi Formation, and 30 from the He 8 member. The results of the parameter calculations are shown in Figure 2; Table 1. The median pressure and range of maximum mercury intrusion saturation in the Upper Paleozoic reservoirs were quite broad, with an above-average mean sorting coefficient. This indicated poor sorting of the reservoir pore sizes, a dispersed distribution, and strong reservoir heterogeneity. According to the capillary pressure curve theory, P_d (displacement pressure), P_{50} (pressure at 50% mercury saturation), and r_{50} (pore-throat radius at 50% mercury saturation) can represent the distribution of pore-throat sizes. In general, the smaller the P_d, the lower the P_{50}, and the larger the P_{50}, the higher the density of the rock (inclined to fineness). Although the oil can be produced, the production capacity is extremely small. The smaller the P_{50}, the better the rock permeability, and the higher the production capacity. r_{50} is the pore radius corresponding to the saturation median pressure P_{50}, which reflects the total pore channel size affected by the physical and chemical origin of the rock and any subsequent changes. S_{Kp} (skewness) and S_p (pore-throat sorting coefficient) can indicate pore-throat sorting. S_p is a measure of the standard deviation of pore channel size in a sample, which directly reflects the concentration of pore channel distribution. In the total porosity, when the pore channel with a certain grade is dominant, it indicates that the pore sorting degree is good. The smaller the S_p value, the more uniform the pore distribution, and the $S_p > 0$. S_{Kp} is a measure of the asymmetry of pore channel size distribution. The S_{Kp} value varied between ±1, that is, $-1 \leq S_{Kp} \leq 1$; $S_{Kp} = 0$, indicating that the pore distribution curve is symmetrical, $S_{Kp} > 0$ is coarse

TABLE 1 Classification and statistics of pore structure parameters.

Stratum	P_{50}/MPa	r_{50}/μm	S_p	P_d/MPa	S_{Hg}/%	W_e/%	S_{kp}
He 8	3.48–35.61	0.02–0.51	1.13–1.84	0.65–2.78	58.46–86.57	33.37–51.82	−1.23–0.55
	11.58	0.16	1.30	1.39	77.85	40.10	0.08
Shanxi	10.65–36.62	0.02–0.07	0.86–1.35	1.54–4.93	55.56–80.01	29.86–40.13	−0.18–1.04
	19.01	0.05	1.21	2.65	70.35	34.94	−0.59
Taiyuan	2.95–4.76	0.16–0.25	0.7–1.41	0.44–0.83	84.2–84.57	37.39–46.61	−0.29–0.37
	3.86	0.20	1.06	0.64	84.39	42.05	0.04
Yanghugou	1.75–23.35	0.22–0.42	1.57–2.06	0.5–1.07	81.98–83.93	11.23–38.67	−4.29–0.49
	4.58	0.24	1.815	0.785	85.96	24.95	−0.4

distortion, and $S_{Kp} < 0$ is fine distortion. S_{Hg} (maximum mercury intrusion saturation) and We (mercury withdrawal efficiency) can reflect pore-throat connectivity. Based on the inverse relationship between pore size and hydrogen nuclei relaxation rates, NMR analysis allows the assessment of fluid distribution within different pore structures by using the transverse relaxation time T2 (Liu et al., 2020). The primary instrument used was the MRIL-C/TP, with a resonance frequency of 2.6 MHz, echo time of 0.6 m, and 1,024 echoes. The wait time was set to 8,000 m, and 32 scans were conducted, ensuring a signal-to-noise ratio above 80:1. High-speed centrifugation was performed on core samples saturated with 100% water at 100 psi (0.689 MPa) to establish the state of the bound water, with the centrifugation process lasting 1 h forward and 30 min in reverse. The microresistivity cast image (MCI) logging method was used to analyze the natural fractures, including their orientations and inclinations. Data acquisition was performed using AC-ME2.1 software, while interpretation was conducted using LEAD2.1 software.

4 Results

4.1 Lithologies

The petrological data indicate (Figures 3, 4) that the Upper Paleozoic tight sandstones in the west mainly comprise quartz sandstone, lithic quartz sandstone, and lithic sandstone. There are certain variances in the types of rocks between the different stratigraphic units.

The Yanghugou Formation consists primarily of grayish-white quartz sandstone (Figures 3A, B) and lithic quartz sandstone (Figures 3C, D). The clastic minerals are dominated by quartz (62.87%), followed by lithic fragments (14.02%), with chert (Figure 3B) and phyllite (Figure 3D) being the main components. The granulometric size of sandstone particles mainly ranges from 0.27 to 0.75 mm, with the maximum grain size of up to 0.95 mm. They are predominantly fine to medium-grained, followed by coarse to medium-grained sandstone. Particle sorting is moderate, with prevalent sub-rounded to subangular shapes, indicating a moderately high degree of textural maturity. The primary types of infill materials are tuffaceous (Figure 3B), kaolinite, siliceous (Figure 3B), and ferruginous minerals, with cement predominantly of the pore-filling type.

The Taiyuan Formation is chiefly characterized by grayish-white quartz sandstone (Figures 3E, F) and lithic quartz sandstone (Figures 3G, H), with the emergence of a small amount of feldspathic lithic sandstone. The quartz content reached 67.04%, whereas the proportion of feldspar remained relatively low at 2.07%. The lithic fragments were predominantly chert (Figure 3F) and metamorphic sandstone (Figure 3H). The grain size ranged from 0.45 to 0.97 mm, with a maximum average diameter of 1.5 mm, mainly medium to coarse sandstone, and is overall moderately to well sorted. The grains were primarily subangular in roundness. The contact types were primarily point lines. The principal infilling materials were illite and siliceous minerals (Figure 3H) with increased relative content, predominantly featuring pore filling and secondary enlargement cementation by minerals.

The Shanxi Formation is predominantly composed of gray-yellow lithic quartz sandstone (Figures 3K, L) and lithic sandstone, with a substantial proportion of feldspathic lithic sandstone and lithic feldspar sandstone (Figures 3I, J). The quartz content was approximately 63.43%, lithic fragments were approximately 17.7%, and the proportion of feldspar increased to approximately 3.21%, mainly comprising metamorphic rock fragments (Figure 3J). This includes sedimentary rock fragments, indicating changes in sediment provenance at this time. The grain size mainly ranged from 0.4 to 1.39 mm, characterized mostly by coarse sandstone with moderate sorting. The grains were primarily subangular to sub-rounded in terms of roundness. The predominant mode of contact is line contact. The main infilling materials are illite, siliceous, and kaolinite minerals, with pore-filling being the primary cementation type.

The He 8 member is dominated by gray lithic quartz sandstones (Figures 3M, N), followed by lithic sandstones (Figures 3O, P) and feldspathic quartz sandstones. The quartz content accounted for 69.12%, with feldspar at approximately 3.97%, and lithic fragments at 15.8%, mainly consisting of metamorphic rock fragments (Figure 3P). The grain size predominantly ranged from 0.42 mm to 1.78 mm, chiefly coarse-grained to pebbly, with

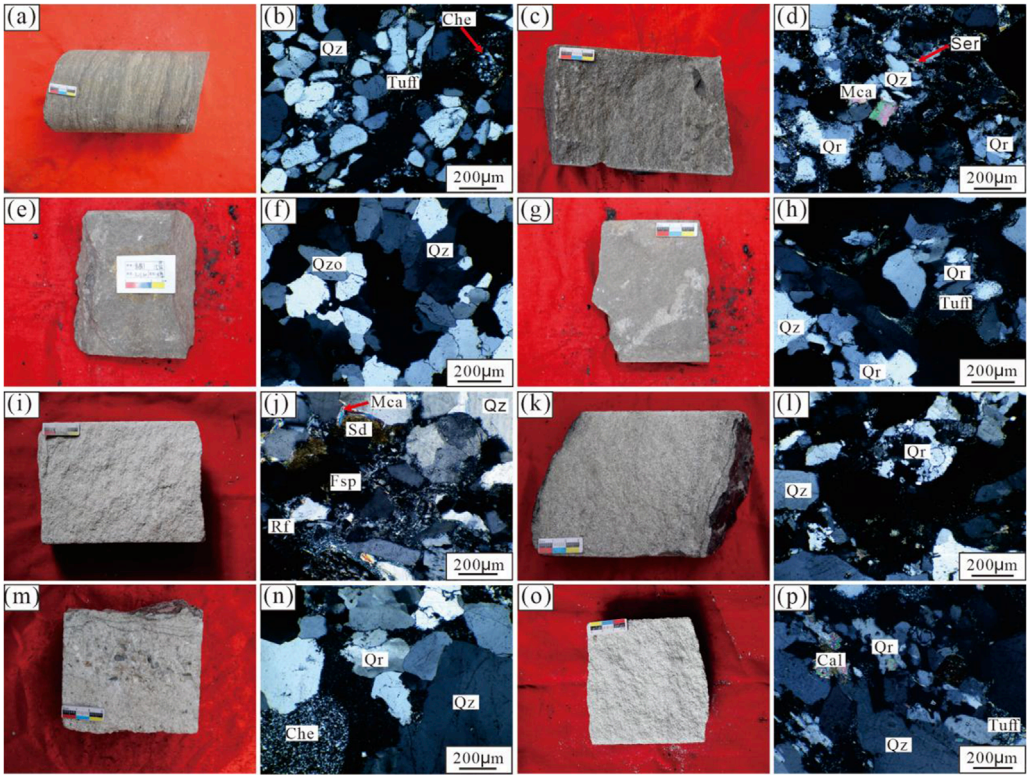

FIGURE 3
Core samples from the Upper Paleozoic of the western Ordos Basin and corresponding microscopic features. **(a)** Gray fine sandstone with wavy bedding (2,597 m, Yanghugou Formation, Well YT2). **(b)** Microscopic photograph of the sample from Fig. **(a)**. Tuffaceous inequigranular quartz sandstone; detrital components are predominantly quartz, with quartzite and flint fragments, showing an oriented arrangement. **(c)** Grayish-black medium-grained sandstone with low-angle cross-bedding (3,347.24 m, Yanghugou Formation, Well AC1). **(d)** Microscopic photograph of the sample from Fig. **(c)**. Argillaceous fine to medium-grained lithic quartz sandstone, with detrital components mainly of quartz and quartzite, with sericite and minor carbonate minerals as filling material. Plastic components are strongly deformed. **(e)** Grayish-white coarse-grained sandstone (4,116.6 m, Taiyuan Formation, Well HT1). **(f)** Microscopic photograph of the sample from Fig. **(e)**. Siliceous coarse-grained quartz sandstone, with detrital components mainly quartz, with common enlargement of quartz grains. **(g)** Gray medium-grained sandstone (4,115.1 m, Taiyuan Formation, Well HT1). **(h)** Microscope photograph of the sample from Fig. **(g)**. Argillaceous inequigranular lithic quartz sandstone, with detrital components mainly of quartz and quartzite, and filling material predominantly altered tuffaceous material. **(i)** Gray-yellow coarse-grained sandstone (3,097.5 m, Shanxi Formation, Well E101). **(j)** Microscopic photograph of the sample from Figure **(i)**. Contains altered tuffaceous medium to coarse-grained feldspathic lithic sandstone, with detrital components of quartz, feldspar, acidic pyroclastic fragments, and mica, and filling material composed of mica matrix and siderite. Feldspar dissolution is common, with siderite filling the pores and replacing detrital particles. **(k)** Grayish-green medium-grained sandstone with parallel bedding (3,087.44 m, Shanxi Formation, Well YT2). **(l)** Microscopic photograph of the sample from Figure **(k)**. Medium-grained lithic sandstone, with detrital components consisting of quartz and quartzite, with deformation of plastic lithic fragments, and fracturing and dissolution of feldspar. **(m)** Conglomeratic sandstone with basal scour structures (3,713.3 m, the He 8 member, Well E19). **(n)** Microscopic photograph of the sample from Fig. m. Gray lithic arenaceous conglomerate, containing quartz pebbles, flint, and quartzite fragments. **(o)** Grayish-white coarse-grained sandstone with parallel bedding (3,782.8 m, He 8 member, Well E74). **(p)** Microscopic photograph of the sample from Figure **(o)**. Contains altered tuffaceous coarse-grained lithic quartz sandstone, with detrital components of quartz and quartzite, oriented distribution of detritus, with filling material composed of altered tuffaceous matter (Cal, Calcite; Che, Flint; Qz, Quartz; Rf, Rock fragments; Qr, Quartzite fragments; Fsp, Feldspar; QzO, Overgrowth quartz; Qa, Authigenic quartz grains; Dol, Dolomite; Chl, Chlorite; Kln, Kaolinite; Ill, Illite; Tuf, Tuffaceous; Sd, Siderite; Glt, Glauconite; Mc, Microcline; Mca, Mica; Ser, Sericite).

moderate sorting. The roundness was mainly subangular to subrounded, with line contacts being predominant. The primary infilling materials were clay minerals, siliceous rocks, carbonate rocks, and tuffaceous rocks, with pore filling as the main cement type.

Quartz sandstone is the dominant rock type and largely composed of monocrystalline quartz. From the older to younger stratigraphic layers, the proportion of quartz sandstone gradually decreased, whereas the proportions of lithic quartz sandstone and feldspathic lithic sandstone increased. During the Shanxi Period, the content of lithic fragments was at its highest, predominantly consisting of metamorphic and igneous rock fragments, with a lower occurrence of sedimentary rock fragments.

The primary constituents of the infill are kaolinite, illite, siliceous, and carbonate minerals, with the content of kaolinite gradually increasing from older to younger stratigraphic layers. Meanwhile, the abundance of illite was substantial but diminished (Figure 3C), and the content of other infill components remained relatively stable. The tuffaceous content in the Yanghugou Formation was relatively high, whereas it was low in other stratigraphic units.

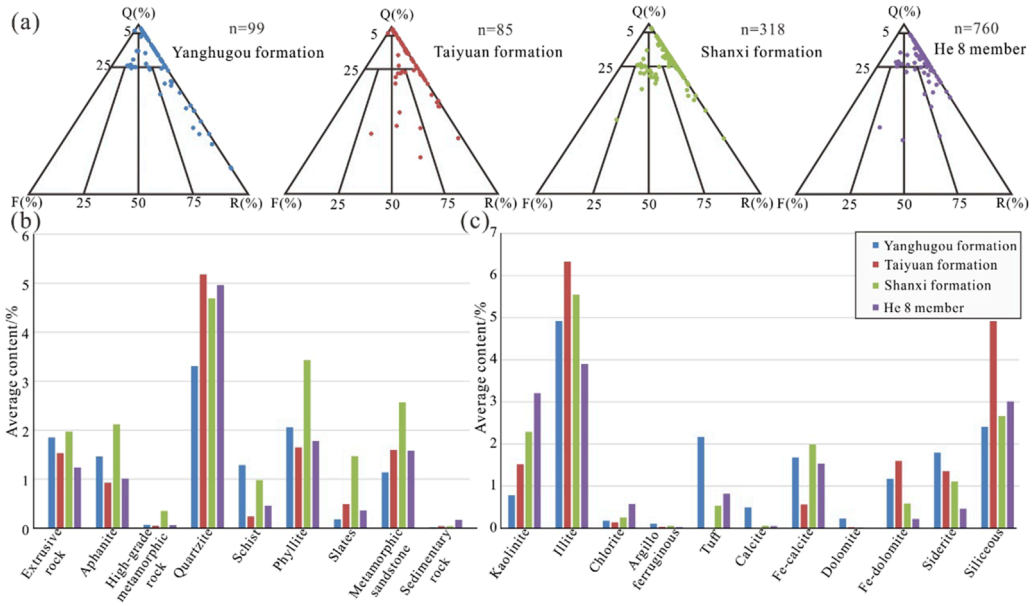

FIGURE 4
Petrological composition of Upper Paleozoic tight sandstone reservoirs. **(a)** Classification of sandstones using Folk's (1968) system. **(b)** composition and content of rock fragments. **(c)** composition and content of pore filling materials.

Grain size analysis indicated that the Upper Paleozoic sandstone clastic particles ranged from 0.27 to 1.78 mm. They primarily consist of medium to coarse sandstone, with a gradual increase in particle size from the older to the newer layers, especially with conglomerate sandstone predominantly in He 8. The particles were moderately well-sorted, and the rounding was primarily subangular. The Yanghugou Formation is characterized by strong hydrodynamic conditions and mainly sub-rounded particles. Textural maturity ranged from submature to mature, with linear and sutured contacts being dominant. The main cementation types were pore filling and secondary enlargement cementation.

4.2 Pore types

Observations from 645 thin sections indicated that the primary porosity was mainly due to unfilled intergranular pores (23.7%), followed by secondary porosity. This includes dissolution pores (interparticle dissolution pores, 11.07%; feldspar dissolution pores, 9.74%; lithic dissolution pores, 29.72%; and matrix dissolution pores, 1.52%), intercrystalline pores (21.85%), and microfracture porosity (2.32%). The main types of porosity in each stratigraphic unit are different (Figure 5). The Yanghugou Formation mainly has intergranular pores, accounting for 29.59%. The Taiyuan Formation is dominated by debris dissolution pores, accounting for 40.8%. The Shanxi Formation is also dominated by debris dissolution pores, with a proportion of 30.1%. The He 8 member is primarily characterized by intercrystalline pores, accounting for 29.9%. This reflects the complex diagenetic fluid evolution experienced by tight sandstone reservoirs, indicating differences in diagenetic processes. They are the main controlling factors of reservoirs across the different strata of the Upper Paleozoic.

4.2.1 Residual intergranular pores

This porosity type refers to the voids formed between mutually supportive grains during sedimentation, characterized by their cleanliness and regular polygonal shapes. Thin-section data analysis indicated that the average porosity of the intergranular pores within the different strata of the Upper Paleozoic in the Ordos Basin was 0.44% for the Yanghugou Formation, 0.37% for the Taiyuan Formation, 0.16% for the Shanxi Formation, and 0.35% for the He 8 member. The Yanghugou and Taiyuan Formations exhibit the highest frequencies of intergranular pore samples at 29.59% and 27.49%, respectively (Figure 5). Intergranular pores primarily comprise two categories: residual pores enlarged by secondary quartz and infilled with microcrystalline quartz (Figure 6A) and original residual intergranular pores enveloped by clay minerals such as kaolinite and illite (Figure 6B).

4.2.2 Intergranular (intragranular) dissolution pores

Influenced by organic acids from widespread hydrocarbon generation from Permian coal-bearing source rocks in the Ordos Basin, detrital minerals, the clay matrix, and soluble components, such as tuff, directly dissolve to create secondary porosity. Alternatively, secondary dissolution porosity is indirectly formed by the early diagenetic replacement of less soluble siliceous minerals by other minerals, followed by dissolution. Based on their genesis, the dissolution pores include honeycomb-like erosional pores within or between clastic particles (Figure 6E), embayment-shaped erosional pores in quartz particles and authigenically enlarged quartz (Figure 6C), feldspar dissolution pores (Figure 6D), matrix dissolution pores (Figures 6D, I), and a limited number of indirect erosional pores resulting from the later dissolution of quartz replaced by early carbonates (Figure 6F). Lithic dissolution pores

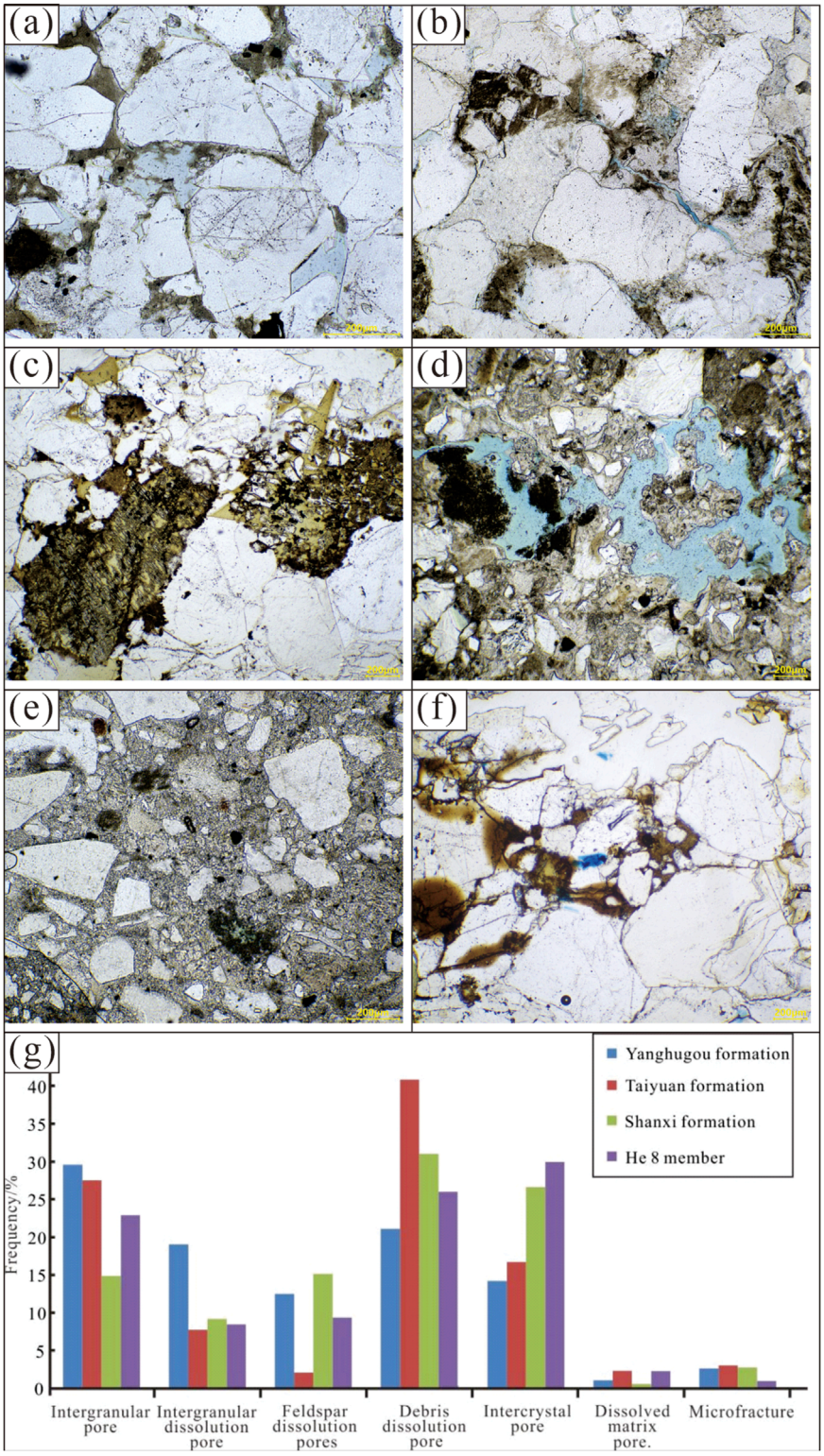

FIGURE 5
Different types of pores characteristics of tight sandstone in western Ordos Basin. **(a)** Quartz is generally enlarged, altered tuff fills part of the pores, and precipitates a small amount of granular rutile, with residual intergranular pores and intergranular dissolved pores, and single polarizing light. **(b)** There are irregular micro-cracks, quartz is common, clay micropores and cuttings dissolved pores, the pores filled with organic matter, single polarized light. **(c)** Quartz is common, feldspar and debris dissolution is strong, with a small number of remaining intergranular pores, feldspar and debris dissolution holes, single polarization. **(d)** There are irregularly dissolved pores, the dissolved matter is altered tuff, part of the debris is sharp angular, single polarized light. **(e)** The debris sorting and grinding are poor, and the intercalation is composed of heterobasic and silty sand, and some of the debris is sharp and angular, with single polarization. **(f)** Visible light oil filling part of the pores, single polarized light. **(g)** Pore type distribution in Upper Paleozoic tight sandstone reservoirs.

were developed throughout the Upper Paleozoic stratigraphic units, with sample frequencies of 21.11%, 40.8%, 30.10%, and 25.96%, respectively. Feldspar dissolution pores primarily contributed to reservoir construction within the Shanxi Formation, with an observable sample percentage of 15.13% (Figure 5). Intergranular dissolution pores developed more extensively in the Yanghugou Formation, with a sampling frequency of 19.03%.

4.2.3 Intercrystalline pores

Intercrystalline pores are primarily formed during diagenesis and develop between authigenic minerals within the pore spaces. The larger the crystal volume, the greater the development of intercrystalline porosity (Han et al., 2019). There has been widespread development of kaolinite and illite intercrystalline pores in the study area. Authigenic kaolinite crystals are pure and coarse, forming hexagonal book-like aggregates under scanning electron microscopy, with larger pore sizes ranging from 5 to 25 μm (Figures 6G, 9K). Illite crystals are fine-grained and polymorphic, exhibiting hair-like, curled lamellar, fibrous forms, with particle sizes typically below 2 μm (Figures 6G, 9J). Compared with other strata, the Shanxi Formation exhibited a higher frequency of intercrystalline pore samples (26.62%), but this did not significantly increase the porosity (Wei et al., 2022).

4.2.4 Fractures

Microfractures have apertures less than 0.1 mm in size and are primarily caused by compaction, shrinkage, and various tectonic stresses. Fractures induced by tectonic stress tend to be relatively fine and straight (Figure 6H). They often penetrate plastic rock debris and the matrix and are relatively clean inside, with a minority filled with argillaceous and siliceous minerals. Shrinkage fractures are widely present in sandstones and are predominantly located within pore-filling clay minerals, that is, montmorillonite and illite. These clay minerals lost bound or structural water during diagenesis, resulting in the contraction toward detrital grains and the formation of linear shrinkage fractures (Figure 6I).

4.3 Porosity and permeability

Analysis of petrophysical data from the study area indicates that overall, the porosity of most Upper Paleozoic samples ranged from 0% to 10%, categorized as low to extremely low porosity. The reservoir permeability varied widely, mostly less than 0.5 × 10^{-3} μm^2, signifying low permeability to tight reservoirs. The porosity of the He 8 member ranged from 0.9% to −18.44%, with an average of 6.81%. The permeability ranged from 0.002–775.6 × 10^{-3} μm^2, with an average of 3.1 × 10^{-3} μm^2. It primarily consists of low porosity to low permeability reservoirs, with some development of medium- and medium-permeability pores, and the least proportion of tight pores. The Shanxi Formation exhibits a higher proportion of extremely low porosity and a higher proportion of tight pores. Porosity ranged from 0.65% to 13.43% with an average of 5.52% and permeability from 0.004–39.63 × 10^{-3} μm^2 with an average of 0.31 × 10^{-3} μm^2. It is primarily characterized by extremely low to low porosity and low permeability to tight reservoirs. The Taiyuan Formation exhibited a porosity range of 0.36%–11.6%, with an average of 6.0%, and a permeability of 0.004–65.57 × 10^{-3} μm^2, with an average of 1.44 × 10^{-3} μm^2, mainly characterized by low porosity and extremely low permeability to tight reservoirs. The Yanghugou Formation has a porosity range of 0.27%–12.43% with an average of 6.22%, and permeability of 0.002–151.82 × 10^{-3} μm^2 with an average of 0.46 × 10^{-3} μm^2, mainly developing low porosity and low permeability reservoirs, comprising the highest proportion of tight reservoirs (Figures 7A, B). Correlation analysis showed that in the western region of the Ordos Basin, the Upper Paleozoic reservoirs had a moderate linear correlation between porosity and permeability indices, with an increase in permeability corresponding to an increase in porosity (Figure 7C). This demonstrates a strong porosity–permeability relationship. Different sandstone reservoir types have distinct petrophysical properties, with feldspathic quartz sandstone exhibiting superior properties compared to other sandstone types (Figure 7D).

The porosity and leakage rate of sandstone in different sedimentary microfacies reservoirs are different. Samples from different sedimentary microfacies were selected for analysis and statistical evaluation of porosity and permeability (Table 2). Within the continental system, that is, the Shanxi Formation + He 8 member, the properties increased in the following order: channel levee/point bar > distributary channel > subaqueous distributary channel > subaqueous river mouth bar/natural levee. Within the transitional marine–continental system, that is, the Taiyuan Formation + Yanghugou Formation, the order was distributary channel/subaqueous distributary channel > barrier sandbar > tidal sandbar > river mouth bar/tidal channel deposits > sand flats. Overall, fluvial facies > plain delta facies > front delta facies.

4.4 Pore-throat size

The median pressures of pore-throat connectivity in the Taiyuan Formation and He 8 member were significantly lower than those in the Shanxi Formation, indicating greater connectivity. The average median pore-throat radius of the Yanghugou Formation was 0.24 μm, and the smallest is in the Shanxi Formation at 0.05 μm; those of other strata were all less than 0.2 μm. Therefore, the pore-throat radii of the Upper Paleozoic reservoirs are concentrated in the micro-throat range, with the presence of a few micro-fine throats.

The Upper Paleozoic reservoirs predominantly exhibited displacement pressures of less than 3 MPa, indicating lower overall displacement pressures. The Shanxi Formation and He 8 member show considerable variability in displacement pressures, with a significant range in the maximum connected pore-throat radii. Meanwhile, the Yanghugou and Taiyuan Formations have relatively lower displacement pressures, with more concentrated maximum connected pore throats. Except for the Taiyuan Formation and He 8 member, which have coarse skewness indicating larger pore throats, the rest had fine skewness. This suggested that the Taiyuan Formation and He 8 member may possess greater oil storage capabilities. The Shanxi Formation has a relatively fine pore-throat distribution with poor sorting, dense lithology, low effective porosity, poor permeability, and low reservoir capacity. The mercury expulsion efficiencies for all layers were below 50%, indicating poor connectivity of the pore throats in tight sandstones. This was related to the small radii of these pore throats. The Yanghugou Formation has larger pore diameters and throat radii than the Shanxi

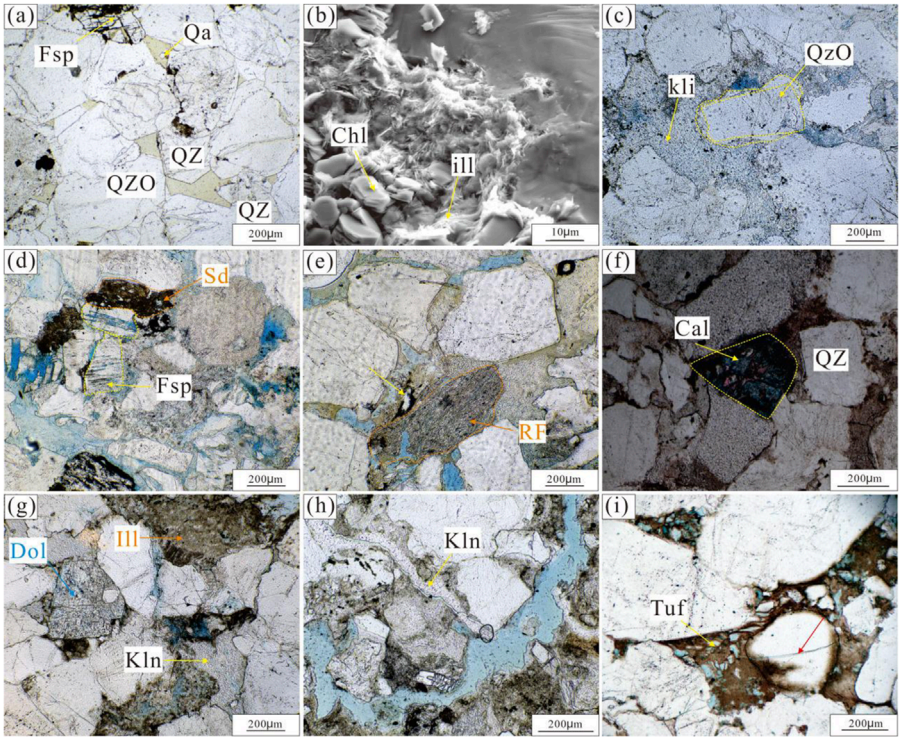

FIGURE 6
Typical pore photographs of the Upper Paleozoic tight gas reservoirs in the western Ordos Basin. **(a)** Quartz enlargement is prevalent, featuring developed remnant intergranular pores, with some feldspar fractured along cleavage (3,893.7 m, Yanghugou Formation, Well E19). **(b)** Intergranular and grain-coating kaolinite and illite clays, along with residual intergranular pores are present (3,753.56 m, the He 8 member, Well E78). **(c)** Edge-related and self-enlargement embayment dissolution is observed at quartz particle margins, with kaolinite infilling the pores. The contact region between kaolinite and enlarged quartz edges is irregular, and there are minor intergranular dissolution pores (3,711.53 m, the He 8 member, Well E103). **(d)** Feldspar dissolution is widespread, with siderite filling the pores and replacing clasts. The primary infill is altered tuff, featuring a few dissolution pores (3,097.5 m, Shanxi Formation, Well E101). **(e)** Clasts exhibit point-line contacts, predominantly consisting of quartz and slate lithic fragments. The infill is composed of altered tuff, with tuff dissolution being common (1,651.1 m, the He 8 member, Well R14). **(f)** Calcite dissolution pores are present (3,489.56 m, Shihezi Formation, Well Z3). **(g)** Sparse intergranular dissolution pores and kaolinite intracrystalline micropores can be observed under plane-polarized light (3,951.2 m, Yanghugou Formation, Well E33). **(h)** Developed structural fractures with associated dissolution, and early-formed fractures filled with authigenic kaolinite can be seen, along with widespread detrital alteration and deformation, under plane-polarized light (4,033.05 m, Shanxi Formation, Well HT1). **(i)** Altered tuff features shrinkage fractures and dissolution pores (4,114 m, Yanghugou Formation, Well HT1).

Formation and the He 8 member. However, due to poor throat width sorting, the mercury expulsion efficiency was lower. In contrast, the Taiyuan Formation had relatively uniform throat radii and widths, greater sorting, higher effective porosity, and the highest mercury expulsion efficiency among the formations studied. Consequently, the reservoir quality was ranked as follows: Taiyuan Formation > He 8 member > Yanghugou Formation > Shanxi Formation.

4.5 Fluid saturation

Overall, the NMR data indicated that the average movable fluid saturation of the Upper Paleozoic strata was 36.79%. In NMR experiments, each layer of the Upper Paleozoic strata exhibited a bimodal distribution. As permeability increased, the amplitude of the right peak of the entire layer increased. This indicated enhanced content and connectivity of large pores (Xiao et al., 2017). This indicates a positive correlation between permeability and NMR porosity (Figures 6A–D). The throat radius and structural characteristics of low permeability reservoirs constrain the characteristics of movable fluid reserves (Zheng and Liu, 2015). The average movable fluid saturation was 49.7% for conglomerate sandstones, 46.0% for coarse sandstones, 38.2% for medium sandstones, and 31.8% for fine sandstones (Figure 8E). There were variations in the NMR experimental results across the different strata. The average movable fluid saturation was 35.8% for the Yanghugou Formation, 46.7% for the Taiyuan Formation, 29.8% for the Shanxi Formation, and 43.18% for the He 8 member. Therefore, the experiments reflect a relatively suitable micropore structure in the Taiyuan Formation and the He 8 member (Figure 8F).

5 Discussion

5.1 Diagenetic evolution

5.1.1 Diagenetic process types

Owing to protracted burial, the Paleozoic strata have undergone complex diagenetic evolution, leading to various types of diagenetic processes. Among them, compaction, cementation, and dissolution

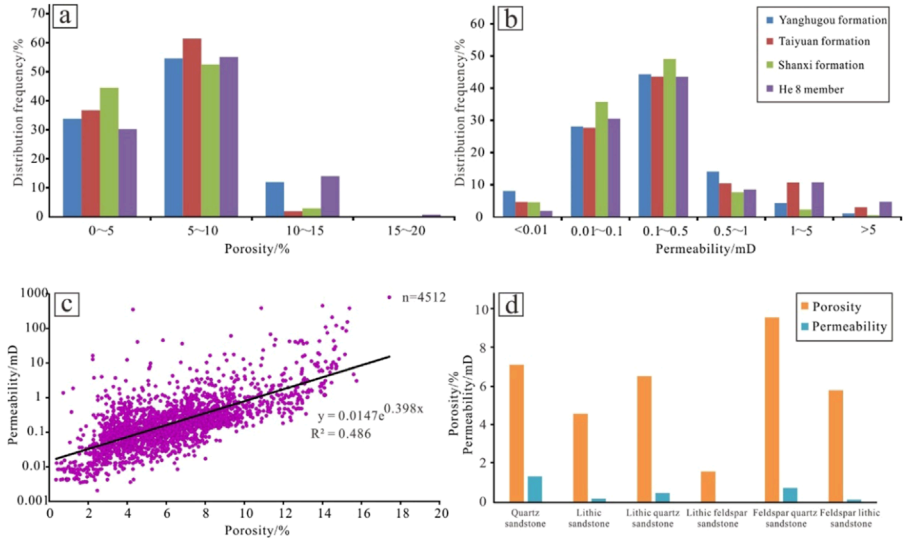

FIGURE 7
Porosity and permeability of tight gas reservoirs in the Upper Paleozoic of the western Ordos Basin. **(a)** Porosity distribution frequency. **(b)** Permeability distribution frequency. **(c)** Porosity-Permeability relationship plot. **(d)** Porosity and permeability of different rock types.

exerted the most significant influence on reservoir properties. Comparing the results with other studies on sandstone porosities due to compaction, which generally decrease below 20% at depths exceeding 3,000 m (Lee et al., 2020).

Compaction: The Paleozoic strata in the western Ordos Basin have been buried at depths exceeding 3,000 m since the mid-Jurassic period and are subject to intensive compaction processes. This has resulted in a substantial reduction in primary porosity, as evidenced by the deformation and twisting of plastic particles. Particles exhibit concavo-convex and suture line contacts (Figure 6A), with rigid particles embedded in plastic particles, consequently diminishing the pore space (Figures 9E, F). The mechanical fragmentation of particles, such as lithic fragments and feldspars, is visible under a microscope, indicative of compaction effects. Compaction has a more significant impact on lithic sandstone and lithic quartz sandstone than on quartz sandstone, with quartz sandstone showing superior resistance to compaction. Therefore, the compaction and pressure solution effects are more prominent in the Shanxi Formation and He 8 member.

Cementation: The primary types of cementation are siliceous and carbonate cementation, with occasional cementation by clay minerals.

Siliceous cement primarily manifests as a substantial secondary enlargement of quartz and a small amount of authigenic microcrystalline quartz aggregates. The development of secondary enlargement of quartz occurs in three stages (Chen, 1990; Li et al., 2015; Su et al., 2021; Zhang et al., 2022). Stage I: During hydrocarbon generation by source rocks, accompanied by the release of abundant organic acids, volcano-like embryonic crystals regrow in a core style on basal crystals, with a limited width of less than 10 μm. The enlargement edges are discontinuous with signs of dissolution, occupying minimal porosity space and formed during the early diagenetic stage B (Figure 9A). Stage II: Quartz growth unevenly encloses quartz grains, forming idiomorphic crystals, with growth margins approximately 15–30 μm wide, partially obstructing porosity. Stage III: In an acidic pore water environment, lithic fragments and feldspars are A (Figure 9B). Stage III: In an acidic pore water environment, lithic fragments and feldspars are dissolved, providing sufficient siliceous material. If there is sufficient porosity, the secondary growth enlargement of quartz from Stage II expands, forming completely polyhedral quartz. Dust lines from the first two stages can be observed under the microscope (Figure 9C), with widths of approximately 15–55 μm, occurring during mesogenetic stage B. In the Yanghugou Formation–He 8 member, the secondary enlargement of quartz and the increase from siliceous influence were especially prevalent, including stage III quartz enlargement in the Shanxi Formation–He 8 member.

Carbonate cement mainly consists of (ferroan) calcite and (ferroan) dolomite, with minor amounts of siderite and glauconite. Cementation can be divided into three stages based on the petrological characteristics of carbonates. Stage I consists of early poikilitic bright crystalline calcite exhibiting ground-mass-style cementation, in which feldspar remains largely undissolved, and compaction is weak. It primarily developed during syngenetic diagenetic stage B (Figure 9D) (Liu et al., 2014). It is predominantly found in the Yanghugou Formation, with limited development in the Shanxi Formation and He 8 member. Stage II is characterized by the formation of organic acids from coal-measure source rocks that dissolve feldspar and lithic fragments. These acids are buffered to a weakly alkaline state, under which small-scale ferroan calcite forms within the tight sandstones. Isotopic analyses (Song et al., 2020) confirmed that Stage II primarily occurred during mesogenetic stage A, with a widespread presence in the Shanxi Formation (Figure 9E). Stage III involves tectonic uplift, where bright crystalline calcite develops along dissolution-induced fractures in grains, sometimes crosscutting mineral particles (Figure 9F), related to late-stage basin uplift and atmospheric freshwater inorganic carbon sources. Siderite mainly occurs in nodular forms, with

10.3389/feart.2025.1523033

TABLE 2 Petrophysical characteristics of Upper Paleozoic reservoirs in different depositional environments in the western Ordos Basin.

Stratum	Sedimentary subfacies	Sedimentary microfacies	Lithology	Porosity/%	Permeability/ 10^{-3} μm^2
He 8	Alluvial plain	Mid-channel bar	Poorly sorted conglomerate, gravel sandstone, and variegated mudstone	4.48–12.94	−2.85–0.0
				8.74	0.69
He 8	Braided River Delta Plain	Distributary channel	Gray-white thick-bedded coarse sandstone, gravelly coarse sandstone	5.25–10.32	0.07–1.05
				7.63	0.42
He 8	Braided River Delta Plain	Nature levee–Crevasse splay	Medium sandstone intercalated with silty sandstone and mudstone	3.94–7.86	0.04–0.65
				6.81	0.28
He 8	Braided River Delta front	Underwater distributary channel	Gray medium sandstone	1.48–14.10	0.04–2.21
				7.39	0.4
He 8	Braided River Delta front	Mouth bar	Gray-white fine sandstone, siltstone	1.45–10.03	0.01–0.12
				7.04	0.07
Shanxi	Alluvial plain	Point bar	Gravelly coarse sandstone	4.28–11.44	0.08–5.58
				7.82	0.62
Shanxi	Meandering river delta plain	Distributary channel	Gravelly coarse-grained quartz sandstone	4.66–10.92	0.05–0.97
				7.28	0.24
Shanxi	Meandering river delta plain	Natural levee–Crevasse splay	Fine sandstone intercalated with siltstone and mudstone	2.80–8.69	0.03–0.50
				5.66	0.38
Shanxi	Meandering river delta front	Underwater distributary channel	Gray gravelly coarse-grained quartz sandstone	2.80–9.10	0.06–0.38
				6.11	0.16
Shanxi	Meandering river delta front	Mouth bar	Gray fine sandstone, Siltstone	2.18–7.38	0.11–0.36
				5.04	0.24
Taiyuan	Tidal delta plain	Distributary channel	Gray-brown medium sandstone, mixed with carbon debris	3.97–10.12	0.60–0.81
				8.31	0.71
Taiyuan	Tidal delta front	Underwater distributary channel	Medium to coarse-grained quartz sandstone	7.09–8.72	0.25–0.65
				7.92	0.39
Taiyuan	Intertidal zone	Sand flat	Brown argillaceous siltstone	2.72–5.49	0.01–0.24
				4.41	0.07
Taiyuan	Barrier island	Barrier sand bar	Medium-grained quartz sandstone	4.85–10.00	0.02–0.47
				7.39	0.25
Yanghugou	Tidal delta front	Underwater distributary channel	Medium–coarse lithic quartz sandstone	11.8–16.4	0.26–1.88
				14.49	0.65
Yanghugou	Tidal delta front	Mouth bar	Well-sorted medium–fine-grained sandstone	1.40–8.66	0.07–0.61
				6.23	0.35

(Continued on the following page)

TABLE 2 (*Continued*) Petrophysical characteristics of Upper Paleozoic reservoirs in different depositional environments in the western Ordos Basin.

Stratum	Sedimentary subfacies	Sedimentary microfacies	Lithology	Porosity/%	Permeability/ 10^{-3} μm^2
Yanghugou	Estuary	Tidal sand bar	Medium–coarse sandstone with argillaceous intercalation	3.59–10.27	0.02–0.75
				7.06	0.40
Yanghugou	Intertidal zone	Sand flat	Fine sandstone with thin layers of mudstone	2.24–3.49	0.01–0.12
				2.88	0.03
Yanghugou	Subtidal zone	Tidal channel	Medium–coarse sandstone with multiple argillaceous laminae	3.38–9.68	0.01–0.66
				6.52	0.23
Yanghugou	Barrier island	Barrier sand bar	Gray coarse-grained argillaceous lithic quartz sandstone or quartz sandstone	5.96–11.34	0.15–1.65
				8.67	0.53

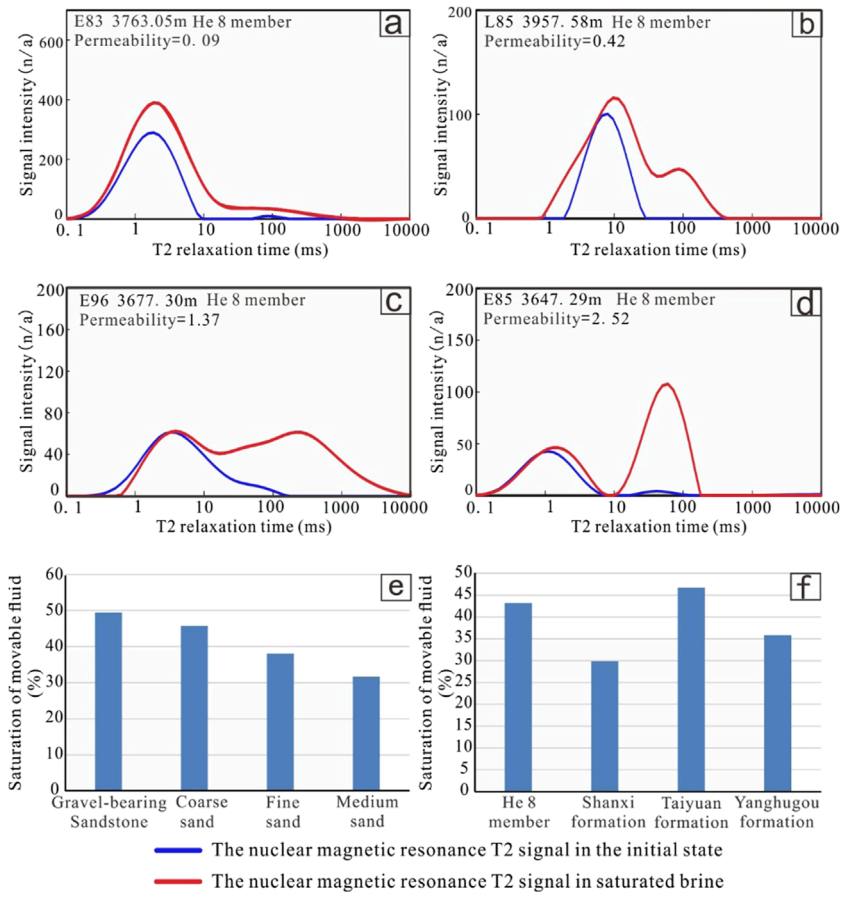

FIGURE 8
NMR testing parameters under different conditions. **(a)** Signal intensity at a depth of 3763.05 m. **(b)** Signal intensity at a depth of 3957.58 m. **(c)** Signal intensity at a depth of 3677.30 m. **(d)** Signal intensity at a depth of 3647.29 m. **(e)** Saturation of movable fluid of different rock types. **(f)** Saturation of movable fluid of different strata.

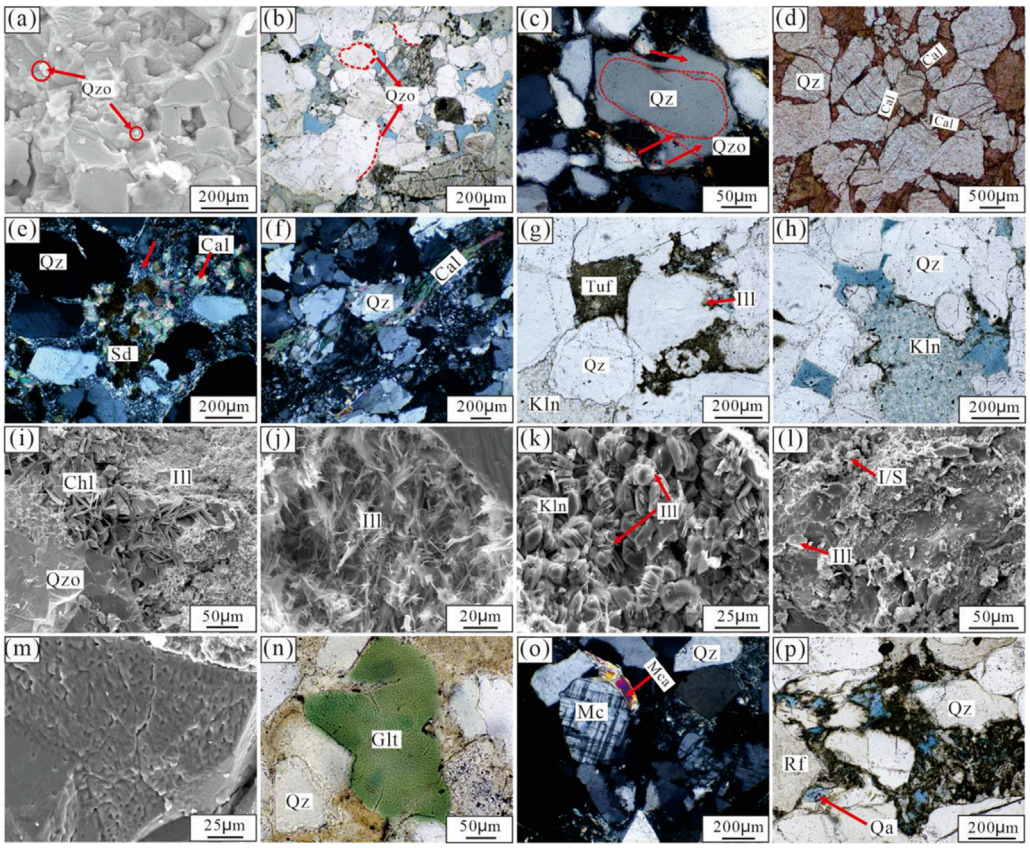

FIGURE 9
Typical diagenetic phenomena in the Upper Paleozoic tight gas reservoirs of the western Ordos Basin. **(a)** Residual intergranular pores following the enlargement of secondary quartz during the first phase (3,812.99 m, Shan 1, Well L34). **(b)** Mixed clast sizes with widespread enlargement of secondary quartz in the second phase, developed intergranular pores, and clay mineral pore filling (2,926.02 m, Yanghugou Formation, Well BC 2). **(c)** Enlargement of quartz observable in three phases (2,598.75 m, Yanghugou Formation, Well YT2). **(d)** Pore filling poikilotopic calcite cement suspending clastic particles (3,643.23 m, the He 8 member, Well MJ1). **(e)** Infills composed of altered tuffaceous material, semi-automorphic microcrystalline granular calcite, and siderite (2,625.24 m, Yanghugou Formation, Well YT 2). **(f)** Early stage fracture development, common fracturing of rigid grains along fractures, with calcite-filled structural joints (2,435.44 m, Shanxi Formation, Well YT 2). **(g)** General enlargement of quartz, with tuffaceous alteration forming illite and kaolinite (4,114 m, Yanghugou Formation, Well HT 1). **(h)** General enlargement of quartz, and kaolinite filling the pores, with common residual organic matter on the pore walls, including residual intergranular pores and dissolution pores (4,116.6 m, Yanghugou Formation, Well HT 1). **(i)** Third stage of quartz enlargement, intergranular illite, petal-like chlorite and other clay infillings, and residual intergranular pores (3,739.19 m, the He 8 member, Well L30). **(j)** Extremely tight structure with partial clastic illitization (4,089.66 m, Taiyuan Formation, Well QT 6). **(k)** Altered kaolinite with illite clay infilling the intercrystalline pores (3,951.85 m, Yanghugou Formation, Well E 33). **(l)** Intergranular and grain-surface illite, illite–smectite mixed layers, and other clay minerals with residual intergranular fissures (3,735.51 m, the He 8 member, Well L30). **(m)** Siliceous dissolution resulting in dissolution pores (4,016.45 m, the He 8 member, Well QT6). **(n)** Contains individual clastic glauconite with developed shrinkage fractures within. The glauconite clasts are composed of cryptocrystalline aggregates (2,598.02 m, Yanghugou Formation, Well YT2). **(o)** Spotted slight contact between clasts, widespread feldspar dissolution, with infills composed of altered tuffaceous material (3,097.5 m, Shanxi Formation, Well E101). **(p)** Featuring irregular microfractures, the clastic components are mainly quartz and quartz lithics, with authigenic quartz filling the lithic dissolution pores (3,953.6 m, Yanghugou Formation, Well E33).

specific feldspar grains replaced by siderite (Figures 6D, E). These are predominantly distributed in the Yanghugou Formation with limited occurrence in the Shanxi Formation, formed during the syngenetic–early diagenetic stage A. Present in trace amounts and distributed as detrital grains, glauconite is indicative of syngenetic diagenesis.

The primary clay mineral cement includes kaolinite and illite. One source of kaolinite is the alteration of volcanic ash, as indicated by simulation experiments using tuffaceous interstitial materials (Liu et al., 2017; Wang et al., 2005; Zhou et al., 2001). Under the influence of permeable formation water leaching, metallic elements such as Al^{3+}, Fe^{3+}, and Ca^{2+} can separate, forming impure intergranular silicate clusters with the concurrent formation of dissolution pore spaces. Some tuffaceous interstitial materials are altered to kaolinite clusters. Kaolinite formed by alteration typically has a poor crystalline form, dirty surfaces, and fine grain size. It often retains fine-grained volcanic ash remnants, making it difficult to provide intercrystalline porosity (Figure 9G). This commonly occurs during early diagenetic stage B. Another form occurs during diagenesis, where acidic fluids continuously leach feldspar grains and silica–alumina-rich minerals. When the silicoaluminates reach a certain concentration, kaolinite can precipitate directly, appearing clean under the microscope with a suitable crystalline form and worm-like shape (Figure 9H). This type of kaolinite is mainly

distributed in the Yanghugou–Shanxi formations, associated with well-developed intercrystalline pores.

Illite cementation and filling action were more pronounced in the western areas (Figure 4C), influenced by the rates of dissolution, precipitation, and the degree of system openness. The direct formation of illite from feldspar seldom occurs. Kaolinite minerals are the most authigenic clay minerals associated with the dissolution of feldspar and other aluminosilicates in clastic rock formations. However, in the western Upper Paleozoic, the illite content was higher than that of kaolinite. SEM observations with scanning electron microscopy indicate two primary modes of illite formation (Tian et al., 2022; Zhou et al., 2016). 1) Transformation from montmorillonite, including I/M mixed layers in volcanic materials (temperature <120°C–140 °C), the morphology under the electron microscope mainly presents a bilayer structure, bent flaky, with the aggregates appearing honeycomb-like (Figure 9I). This was most evident in the He 8 member, in which typical I/S layers were visible (Figure 9L). Such illite is almost nonexistent in the Taiyuan Formation due to the lack of volcanic material and is also relatively low in the Yanghugou Formation. 2) Reaction of kaolinite with potassium feldspar under high-temperature burial conditions (temperature >120°C–140°C), which is rapid until the feldspar or kaolinite is exhausted. These are often present as hair-like, fibrous, or ribbon-like structures (Figure 9J). The alteration of kaolinite into illite was evident, with hair-like illite visible on the edges of the kaolinite (Figure 9K). This type of illite is present throughout the Upper Paleozoic, especially in the Yanghugou Formation–Shanxi Formation. Sandstones with high original detrital content and complete pore filling by volcanic ash have low initial permeability, preventing hydrolysis reactions from occurring and hindering the infiltration of acidic fluids later (Chen et al., 2015). Until mesogenetic stage B, kaolinite was transformed into illite under alkaline conditions. The transformation in the older strata was more thorough. Therefore, the illite content was higher in the Yanghugou Formation than in the Shanxi Formation.

Corrosion: The study area has extensive dissolution of potassium feldspar, lithic dissolution, and intergranular dissolution. During the Late Paleozoic, frequent volcanic activity supplied the western basin margin with abundant volcanic and felsic minerals (Lv et al., 2017). The dissolution provided a matrix for forming secondary porosity in the reservoirs, indirectly creating various related secondary pores, such as lithic dissolution pores (Figure 6E), intercrystalline porosity (Figures 9G, I), dissolution fractures (Figure 6I), and tuffaceous dissolution (Figure 6E). The Early Cretaceous thermal anomaly acidic fluid leaching event led to extensive dissolution and disappearance of feldspar within the Upper Paleozoic coal-bearing strata (Liu et al., 2017; Wei et al., 2017). This left only residual plagioclase and minor microcline (Figure 9O), enhancing the storage space in tight sandstone reservoirs. The degree of feldspar dissolution is most profound in acidic environments, resulting in a lower feldspar content in the Yanghugou and Taiyuan Formations than in the Shanxi Formation and the He 8 member. Other dissolution processes primarily involved intergranular spaces of quartz and within lithic fragments (Figures 6C, E), with quartz silicate dissolution commonly occurring in alkaline environments. The dissolution of quartz grain edges forms embayed shapes. The contact edges are irregularly concave–convex and expand to form fractures, as seen in the Taiyuan Formation and He 8 member.

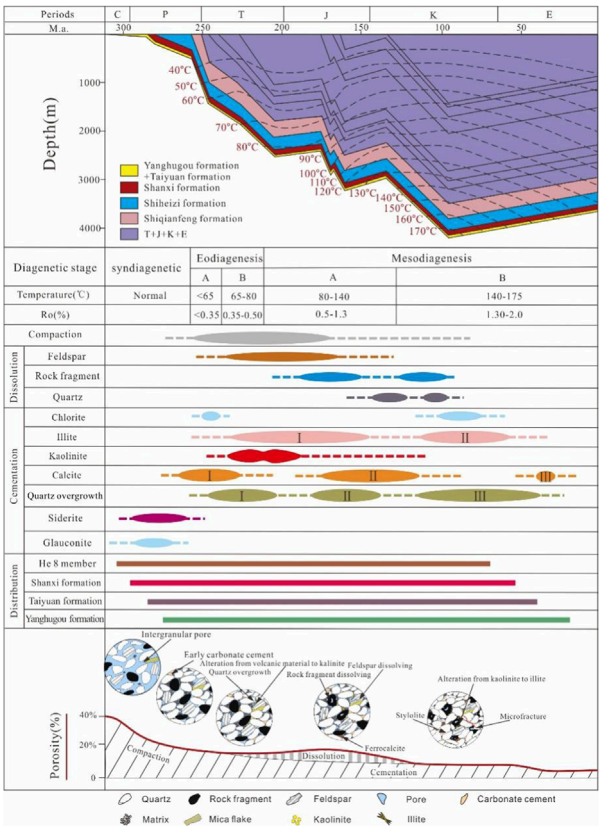

FIGURE 10
Diagenetic evolutionary sequence of the Upper Paleozoic tight gas reservoirs in the western Ordos Basin [adapted from Zhou et al. (2022)].

5.1.2 Diagenetic evolution

Based on burial history studies of the research area (Cao et al., 2015) and according to the clastic rock diagenetic stage classification scheme (Zhou J. S. et al., 2022), diagenesis is categorized into three phases (Figure 10). Considering the diagenetic features, the Yanghugou Formation to the He 8 member is within the syngenetic–mesogenetic diagenetic B phase, with heterogeneity at various stratigraphic levels. In the sandstones of the Yanghugou Formation to the He 8 member, quartz growth was consistently associated with secondary enlargement. The primary carbonate minerals were bright crystalline spar calcites with widespread development of ferroan calcite. The dominant clay minerals are kaolinite and illite, with intergranular contacts predominantly of the point-line type and locally observed suture line contacts. All of these indicate that the stratigraphic levels have generally entered the mesogenetic B phase of diagenesis (Mesodiagenesis refers to the continuous burial process under surface diagenesis, with long time intervals and rather slow pore changes, mainly related to the pressure dissolution of sediments or rocks and the redistribution of materials, recrystallization or metasomatism.). Various diagenetic actions differentially influence the reservoir and may enhance or reduce its petrophysical properties.

Syngenetic diagenetic stage: Freshly deposited and not yet lithified clastic materials steadily subside within the strata and are

influenced by weakly acidic groundwater from volcanic detritus and coal-bearing strata. Diagenesis was weak and primarily involved the hydrolytic alteration of volcanic materials (Figure 6E). Mobile elements readily migrated to form mineral assemblages with the local development of siderite rhombs (Figure 9E) and glauconite precipitation (Figure 9N), particularly within the Yanghugou Formation strata. The grains were primarily in point contact or not in contact with the well-developed original intergranular pores.

Early diagenetic stage A was dominated by mechanical compaction, characterized by point contacts between detrital grains and the deformation of pliable lithic fragments. This included slate and schist (Figure 9O), with local fracturing of rigid minerals also occurring (Figure 9F). Coal-bearing strata are subjected to a strongly acidic fluid environment, initiating the early dissolution of alkali feldspar and lithic fragments, with indications of a pressure solution becoming apparent. An alkaline diagenetic environment prevailed in the He 8 member, with early carbonate cementation commencing (Figure 9D) (Sun et al., 2017). During the early diagenetic stage B, some volcanic materials served as pore-filling substances. In strata rich in potassium feldspar, they facilitated the production of early illite and kaolinite, whereas siliceous cement began to precipitate, further reducing the porosity between grains (Figure 9A).

Mesogenetic stage A: As the basin fluctuated and subsided, coal-bearing strata continued to release organic acids, making dissolution the most important diagenetic process that dissolved feldspars, rock fragments, and early carbonate minerals. With increasing compaction, the grains exhibited linear contacts, leaving behind a small amount of primary residual porosity (Figures 6A, 9H). Feldspars are often replaced by other clay minerals, and intercrystalline pores develop within the new minerals. As vitric alteration releases alkali metal ions and acidic fluids that are consumed over time, the diagenetic environment shifts toward alkalinity. This leads to the secondary enlargement of quartz (Stage II) and the appearance of ferroan calcite (Stage II). Although compaction and cementation continued to destroy the primary porosity during this stage, dissolution and alteration generated many secondary and intercrystalline pores.

Mesogenetic stage B: The iron-rich diagenetic fluids gradually approached alkaline equilibrium, while kaolinite was transformed into illite. This resulted in a relative increase in the illite content. Owing to regional uplift, many microfractures were formed (Figure 9P), and quartz and rock fragments were dissolved (Figure 9M). However, as the burial depth increased, cementation by Fe-rich carbonate minerals and quartz intensified (Figure 9F), filling most of the residual porosity (Zhang et al., 2022).

5.2 Primary controlling factors in the formation of high-quality reservoirs

Provenance and sedimentation are the basis of reservoir formation, and the provenance system causes differences in sand body thickness, reservoir rock types, and physical properties, with different types of sedimentary facies further "preserving and transforming" the structural components of sandstone. Diagenesis further controls the difference of reservoirs in the study area based on provenance and sedimentation, and fractures are the main reason for the high permeability of reservoirs.

5.2.1 Parent rock type

During the Late Paleozoic era, the Alxa ancient land in the northwest, the Yinshan–Yanshan orogenic belt in the northeast, and the Northern Qilian–Qinling orogenic belt in the south emerged as the primary source areas (Han et al., 2014; Wang, 2017). The parent rocks of the Yinshan–Yanshan orogenic belt are predominantly medium to high-grade metamorphic rocks. The Alxa ancient land is characterized mainly by clastic rocks, low-grade metamorphic rocks, and granite. The Northern Qilian orogenic belt is characterized by greenschist schists, slate, and quartzite. The Northern Qinling Orogenic Belt has high-grade metamorphic rocks, magmatic rocks, and a minor amount of sedimentary rocks. Clastic reservoirs based on lithological characteristics can be categorized into two types (Qiu et al., 2019): porosity-increasing clastics, including high-grade metamorphic clastics, quartz clastics, metamorphic sandstone, carbonate clastics, and granite clastics, and porosity-reducing clastics, including volcanic clastics, cryptocrystalline clastics, slate clastics, schist, phyllite, mica clastics, siltstone, mudstone clastics, and chlorite debris. Porosity-increasing clastics underwent extensive internal dissolution along contact fractures under the influence of alkaline fluids, leading to a discernible positive correlation with reservoir porosity (Figure 11A). Porosity-reducing clastics are resistant to dissolution and deformation, occupy space under compaction (Figure 6E), and exhibit a negative correlation with reservoir properties (Figure 11B). According to the nature of the source area parent rocks (Wei, 2002), the Yinshan orogenic belt primarily contributes to porosity-increasing clastics such as gneiss, granulite, and migmatite. The Alxa ancient land mainly yields porosity-reducing clastics such as quartzite and metamorphic sandstone. The Qilian–Qinling orogenic belt is chiefly the source of gneiss, slate, and basalt clastics. This has resulted in distinct reservoir quality variations attributed to the north–south source areas, especially the intense contributions from the north in the Shanxi Formation and the He 8 member. Taking the Shanxi stage as an example, the study area received abundant terrestrial supplies with high sand body thicknesses (Figure 11C). Alxa and Yinshan served as northern material suppliers, whereas the Qilian–Qinling orogenic belt rarely provided materials. Porosity statistics for the west and east parts showed average porosities of 6.39% and 7.05%, respectively, with permeabilities of 0.20×10^{-3} μm^2 and 0.39×10^{-3} μm^2. This suggests that the type of clastic material controlled by the material source governs the evolution of reservoir porosity and final petrophysical properties. Porosity-increasing and porosity-reducing clastics are supplied by the southern material source area, with developed sedimentary clastics, having porosity and permeability of 5.05% and 0.15×10^{-3} μm^2, respectively. These values are lower than those of the northern region, leading to differences in reservoir quality between the north and south. The reservoir quality during other periods was affected by the time and intensity of material supply.

5.2.2 Sedimentary microfacies

The variations in the physical properties of reservoirs across different depositional facies are primarily governed by the sedimentary environment (Aminul Islam, 2009). Hydrodynamic conditions, as controlled by the sedimentary setting, affect the size, sorting, and rounding of clastic particles,

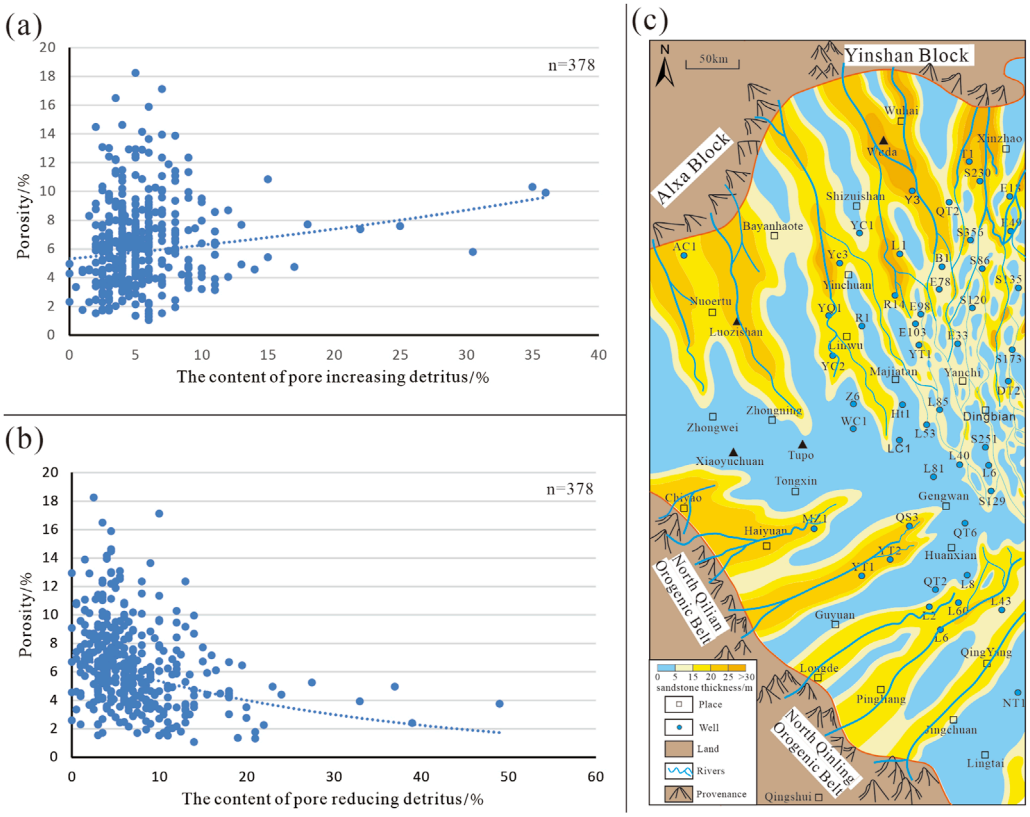

FIGURE 11
Impact of different types of rock fragments on porosity in the tight Upper Paleozoic reservoirs of the western Ordos Basin. **(a)** Relationship between the content of pore increasing detritus and porosity. **(b)** Relationship between the content of pore-reducing detritus and porosity. **(c)** Provenance subdivision and sand body distribution of the Shanxi Formation in the western Ordos Basin.

composition and matrix content. This leads to differences in the original porosity and permeability of the sediments (Dong et al., 2014; Weedman et al., 1992).

In the study area, the Yanghugou Formation sand bodies are primarily developed as barrier islands, subaqueous delta distributary channels, river mouth bars, tidal flats, tidal sandbars, tidal channel deposits, and tidal sand flat depositional environments. The Taiyuan Formation sand bodies are deposited in delta plain distributary channels, delta front subaqueous distributary channels, and barrier sandbars, with a more confined sandbar system development compared to the Yanghugou Formation. The Shanxi Formation sand bodies mainly occur in high-gradient alluvial plain meandering river channels, point bars, natural levees, delta plain distributary channels, and delta front subaqueous distributary channel depositional environments. During the Shihezi stage, active tectonic movements and substantial uplift of the paleo-land area resulted in a more robust progradation of the delta into the lake. Compared to the Shanxi Formation, the delta front facies were more developed, with repeated and overlapping multi-stage river channels promoting the development of thick layers of coarse-grained sand bodies (Tian et al., 2011).

The sedimentary environment controls the sandstone thickness, composition, and depositional extent (Bloch et al., 2002). Sandstone thickness is a critical indicator of the depositional environment. The frequent lateral migration of channels and seasonal variations in river flow have led to the formation of sand bodies of varying types and thicknesses (Tian et al., 2011). Sandstone with a thickness of less than 5 m has petrophysical properties with an average porosity of 4.27% and permeability of 0.17×10^{-3} μm^2 that are inferior to those of sandstones with a thickness of 5–10 m, which has a porosity of 5.66% and permeability of 0.31×10^{-3} μm^2. These values are significantly lower than those of sandstones with a thickness of 10–20 m with a porosity of 6.76% and permeability of 1.49×10^{-3} μm^2. The correlation between rock porosity, permeability, and sand body thickness (Figure 12A) suggests that thicker sand bodies can enhance reservoir development, especially within the Yanghugou Formation. Such thick sand body layers indicate a high-energy depositional environment. They represent the intercrossing, stacking, and compounding of various sand body facies controlled by their respective depositional environments (Yang et al., 2014). The thickness of the sand bodies in the Yanghugou Formation ranges from 2 to 10 m and in the Taiyuan Formation from 5 to 20 m. In the Shanxi Formation, they have shown a gradual increase, concentrated in the 10–20 m range, with the He 8 member centering at 15–25 m. This indicates that the petrophysical properties of the continental depositional system are generally more suitable to those of the marine–continental transitional depositional system (Shen et al., 2022).

The main lithology of the reservoir in the study area is quartz sandstone, with quartz content exceeding 60% in each stratum.

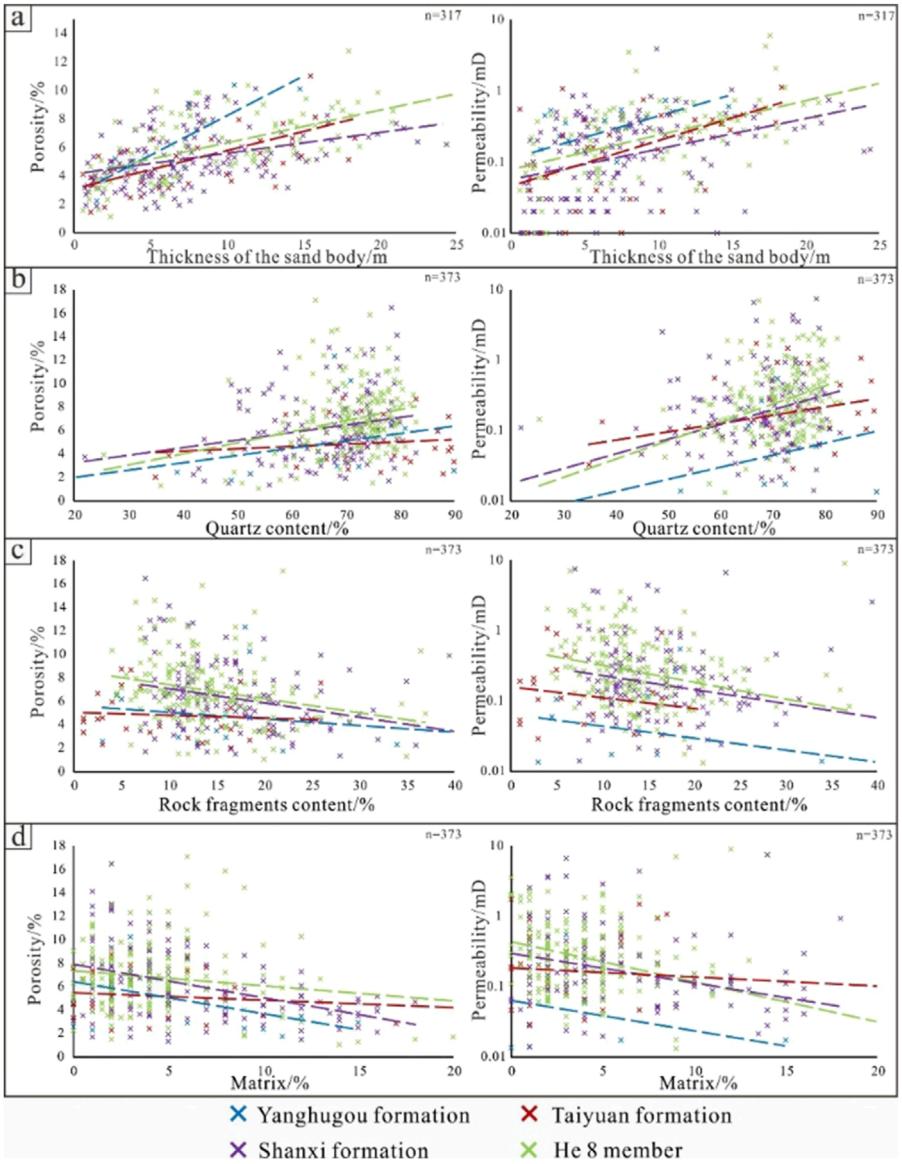

FIGURE 12
Relationships between sedimentary indicators and porosity and permeability. **(a)** Cross-plot of sand body thickness with porosity and permeability. **(b)** Cross-plot of quartz content with porosity and permeability. **(c)** Cross-plot of lithic fragment content with porosity and permeability. **(d)** Cross-plot of matrix content with porosity and permeability.

Quartz grains usually demonstrate strong resistance to compaction, which helps to preserve primary porosity (Weedman et al., 1992). Higher quartz content is correlated with better reservoir quality (Figure 12B). Although feldspar generates secondary porosity during diagenesis, its relatively low content does not substantially enhance the reservoir quality. Other rock particles tend to reduce porosity and permeability during compaction by undergoing cementation and replacement processes that fill the primary pores. Rock fragments have weak resistance to compaction, easily fill primary pores, and lower reservoir quality, especially in the He 8 member (Figure 12C). However, the correlation coefficient was weak. The presence of abundant dissolved pores can increase reservoir porosity and enhance permeability, particularly where the feldspar content is the highest in the Shanxi Formation, making the correlation even weaker. Nevertheless, quartz grains are the most important factor affecting the petrophysical properties of Paleozoic reservoirs. The properties of the quartz sandstone were more suitable than those of the other sandstone types (Figure 7D). The matrix content is an indicator of the structural maturity of sandstones, restricting fluid flow within pores. Diagenetic fluids are less likely to improve pore quality, resulting in a negative correlation between the physical properties of the reservoir and the matrix content (Figure 12D). Characterized by relatively high quartz, low rock fragments, and low matrix content, the Taiyuan Formation and He 8 member form a superior petrophysical foundation.

The grain size of sandstones is also a primary factor affecting the sedimentary reservoir properties, with the average grain

size of the principal Paleozoic sandstones gradually increasing. Grain size and petrophysical property statistics from the western regions indicate that the average porosities of conglomeratic coarse sandstone, conglomeratic medium sandstone, coarse sandstone, medium sandstone, fine sandstone, and siltstone are 8.06%, 5.99%, 5.76%, 4.62%, and 2.34%, respectively. The permeabilities are 0.54 $\times 10^{-3}$ μm^2, 0.23 $\times 10^{-3}$ μm^2, 0.15 $\times 10^{-3}$ μm^2, 0.08 $\times 10^{-3}$ μm^2, and 0.03 $\times 10^{-3}$ μm^2, correspondingly. NMR experiments showed that sandstones with larger grain sizes exhibited more suitable micropore structures (Figure 6E). As the grain size became finer, the parameters from the HPMI tests diminished, indicating a reduction and homogenization of pore throats. This suggests that sandstones with larger grain sizes are prone to more open diagenetic environments during diagenetic evolution, facilitating the expulsion of pore fluids and thereby forming more intergranular porosity and enhanced permeability.

In continental systems, the fluvial facies, distributary channels, and subaqueous distributary channels are primarily composed of medium to coarse sandstone. Owing to substantial variations in hydrodynamic conditions, better sorting, higher structural maturity, higher quartz content, and low clay and matrix contents, along with weak compaction and cementation or increased dissolution, these facies have the most suitable reservoir properties. Despite being well sorted from persistent and stable strong hydrodynamic action, mouth bars/natural levee deposits are primarily fine sandstones with a high matrix content, resulting in poorer reservoir properties. In the marine–continental transitional system, barrier sandbars develop abundant quartz sandstones due to repeated scouring by seawater, meaning that they have the highest reservoir quality. Although sand flats are mainly composed of quartz sandstone, they have a higher matrix content, finer grain size, and the lowest compositional maturity, resulting in the poorest reservoir quality. In tidal channels and sandbar deposits, the primary porosity is easily filled by the argillaceous matrix. Therefore, the quality is poor. The petrophysical properties of the Upper Paleozoic reservoirs on the western margin of the Ordos Basin are strongly controlled by depositional facies, with differences in sedimentary processes primarily reflecting variations in the hydrodynamic conditions of each depositional area. Different depositional facies determine the variations in the reservoir's physical properties (Zhu et al., 2022).

5.2.3 Diagenesis

After the sediments are buried, a series of diagenetic processes related to interactions between sedimentary components, pore water, and diagenetic fluids are initiated due to increases in temperature and pressure. These processes affect the development of pore structures, which can degrade or enhance the quality of the reservoir (Baker, 1991). The cumulative effects of diagenesis substantially alter the composition and structure of sandstones and strongly affect their reservoir properties.

Compaction can be categorized into mechanical and chemical dissolution, which occurs at different burial depths (Figure 13A). The first phase occurs at an approximate burial depth of ~2,500 m and is characterized by early mechanical compaction. Here, increasing pressure leads to the rearrangement of detrital particles into tighter point contacts and the precipitation of authigenic minerals from pore waters into interstitial spaces. This results in a substantial loss of original porosity (Figures 6E, 9O). The second phase occurs between 2,500 and 5,000 m. As the burial depth increased (2,500–4,000 m), the support from rigid particles and cement made further compaction of the detrital particles difficult (Figure 9F). The formation of secondary porosity at this depth slightly enhanced the rock properties. Beyond 4,000 m, the solubility of contact points between rigid particles increases with temperature and pressure, leading to dominant chemical dissolution. This primarily transformed contact modes into sutured and stylolitic contacts and substantially reduced porosity connectivity (Figure 9G). In the Yanghugou Formation, He 8 member, the burial depths are concentrated at 3,500–4,500 m, where chemical dissolution is exceptionally intense. The graphical representation of cement volume to grain volume (Figure 13B) indicates that compaction destroys more original porosity than cementation. Compaction reduced the porosity by a range of 1%–92.5%, averaging 66%, highlighting compaction as the most important factor in degrading the physical properties of the reservoir.

Cementation reduced the porosity within the range of 2.5%–97.5%, with an average reduction of 33%, indicating that cementation is an important factor in sandstone densification. Siliceous cement in tight sandstone reservoirs occurs primarily as secondary enlargements of quartz, with a dual effect on reservoir properties. When the cement content was below 4%, the compressive strength of the rock increased, and the primary pores were protected. At this point, the porosity and permeability are positively correlated. However, the pore throats contract, leading to a decrease in permeability. The Yanghugou Formation to the He 8 member exhibits this distribution. With an increase in the secondary enlargement rim width and contents ranging from 4% to 8%, under the dual diagenetic processes of dissolution in an alkaline environment and pore filling, the correlation between them was not significant. When the content exceeded 8%, pore filling became dominant, with further intensification of the Phase III secondary enlargement of quartz. This affected the densification process of the Yanghugou–Shanxi Formation sandstone reservoirs, with a weaker destructive effect on the He 8 member reservoir (Figure 14A). Commonly observed under microscopy and formed in various stages, carbonate cementation effectively counteracts compaction. Meanwhile, it occupies a considerable volume of reservoir space and blocks pore throats. This is detrimental to the later stages of fluid invasion, leading to reservoir densification. Consequently, sandstones with a high carbonate cement content exhibited lower porosity and permeability, with the primary impact observed in the Shanxi Formation and He 8 member (Figure 14B). The developmental forms and contents of different clay minerals vary, resulting in distinct controlling effects on the reservoir properties of each layer. The genesis, forms of occurrence, and pore-filling patterns of kaolinite contribute to its complex petrophysical relationships. Under a microscope, most kaolinite was derived from feldspar dissolution, fostering the development of dissolution pores. Given that crystals inherently possess intercrystalline pores and have limited filling capacity, the kaolinite content in the study area is positively correlated with porosity but has an indistinct relationship with permeability. The Yanghugou Formation contains less kaolinite with no significant impact on the reservoir, whereas the effect is most pronounced in the He 8 member (Figure 14C).

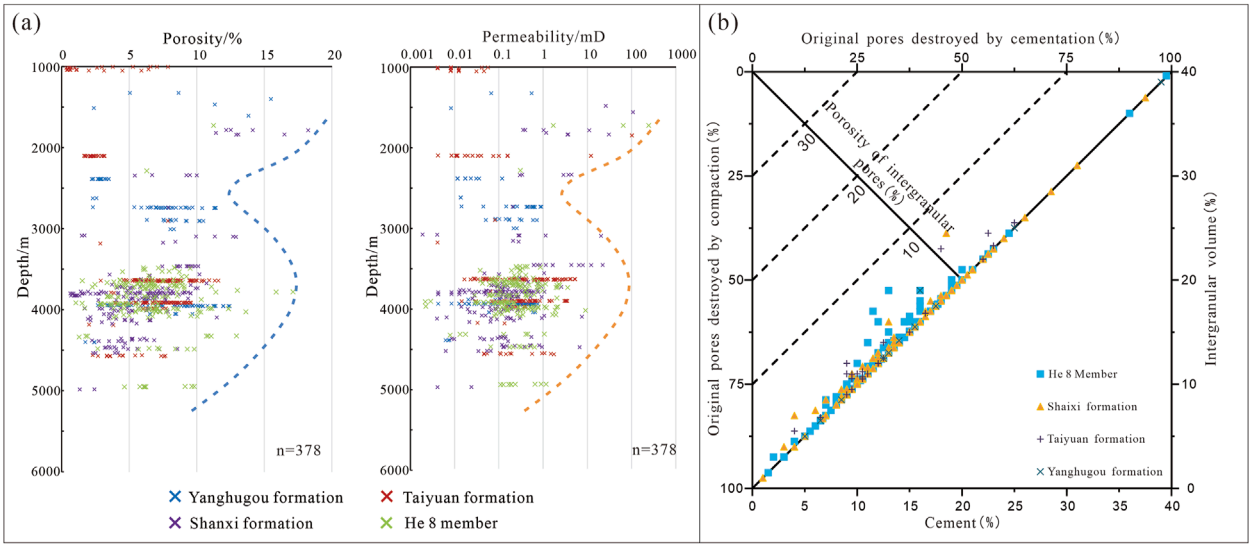

FIGURE 13
Impact of compaction and cementation on porosity in the tight Upper Paleozoic reservoirs of the western Ordos Basin. **(a)** Cross-plot of reservoir depth and porosity–permeability relationships in the Upper Paleozoic reservoirs of the western Ordos Basin. **(b)** Strength analysis of sandstone compaction and cementation to reduce porosity in the study area.

Regardless of its origin, illite tends to form a network-like distribution within the pores, constraining them and resulting in lower petrophysical properties. This can result in manifestations in the petrophysical relationships of both the Yanghugou Formation and the He 8 member (Figure 14D). Chlorite suppresses compaction (Figure 14E) and prevents the destruction of pores by subsequent cementation processes such as quartz enlargement (Figure 9I). It may occupy pores and reduce pore connectivity, with the main expression in the Shanxi Formation–He 8 member. However, owing to its relatively low content (<0.6%), its impact on reservoirs is minimal.

Under strong compaction and cementation, the sandstones were almost devoid of primary intergranular porosity. Thus, dissolution played a critical role in forming sweet spots within the reservoir. The secondary porosity in the reservoirs at various stratigraphic levels originated differently, with the Yanghugou and Taiyuan Formations mainly developing lithic and intergranular dissolution pores. Meanwhile, the Shanxi Formation and He 8 member primarily exhibited lithic and feldspar dissolution pores (Figure 5). The presence of abundant volcanic material in the Yanghugou Formation promoted the extensive dissolution of feldspar. Meanwhile, the depositional environment of the Taiyuan Formation sand bodies, predominantly transitional marine–continental barrier islands with high quartz content, did not favor the development of feldspar dissolution pores. The sand bodies of the Shanxi Formation and He 8 member reservoirs are mainly derived from the subaqueous distributary channels of the delta front, which contain abundant feldspar. Pervasive hydrocarbon generation in coal-bearing strata produces organic acids, leading to the extensive dissolution of unstable particles, such as lithic fragments and feldspar. Organic acids also accelerated the erosion rate of quartz (Guo et al., 2003), resulting in the partial intergranular dissolution of quartz (Figure 6C).

5.2.4 Fracture system

The composition, structure, and diagenetic processes of tight sandstone are crucial for reservoir quality. However, in the west, some tight sandstones with high permeability (>1 × 10^{-3} μm^2) have a weak relationship with these factors and show a low correlation with the depositional and diagenetic processes. This indicates that relatively high-permeability reservoirs are controlled by other factors. The extractive values of low permeability and ultralow-permeability oil and gas reservoirs are closely related to the presence of various structural and nonstructural fractures within the reservoir (Fan et al., 2016).

The thrust fault belt along the western margin began to bulge in the Early Triassic, reached its peak during the Yanshanian period, and became more complex during the Himalayan orogeny. High-permeability areas in the Upper Paleozoic were mainly distributed in structural regions affected by post-depositional Yanshanian and Himalayan movements (Gao et al., 2019; Xia et al., 2005; Zhao et al., 2016). Structural fracture reservoirs have been discovered in structures, such as the Shigouyi and Liujiagou back anticlines (He et al., 2021). This indicates that these reservoirs were controlled by later tectonic movements (Fan et al., 2022). Image logging showed that multiple phases of fractures and faults developed in different layers of the structural belt. Image logging of Well L 61 shows blocky and stratified core structures with high-angle fractures of varying orientations, such as predominantly SW-oriented fractures in the Yanghugou Formation and NW–SE-oriented fractures in the Taiyuan Formation (Figure 15). The structural regions formed by compressive stresses in different directions suggest shallow burial depths and lower overlying stratum pressures that prevented extensive diagenetic damage in later periods. The folding and faulting action in the foreland basin thrust belt forms a network fracture system with infiltration and dissolution by atmospheric freshwater. This plays an essential

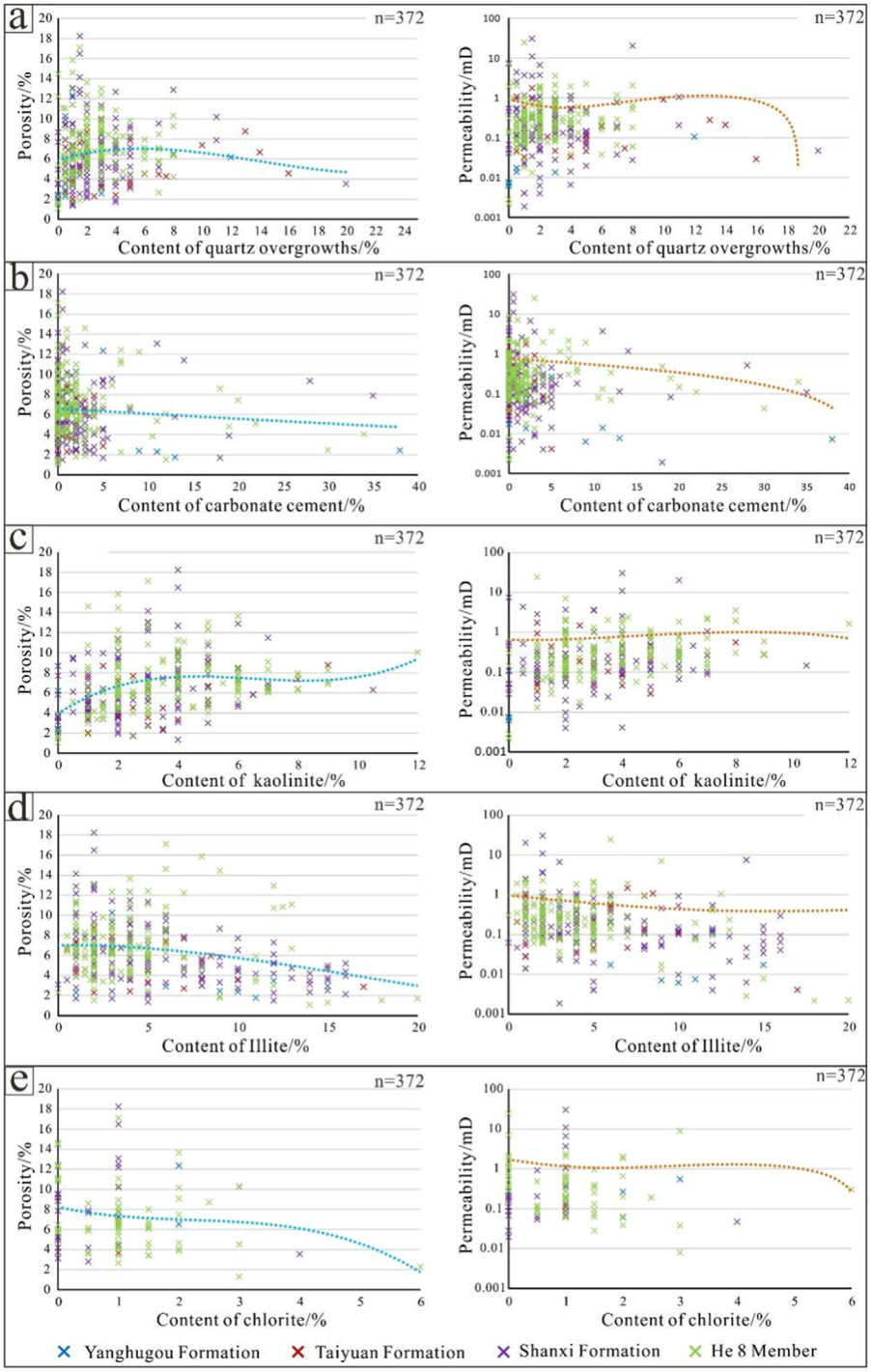

FIGURE 14
Relationship between cement content and porosity/permeability. **(a)** Relationship between content of quartz overgrowths and porosity/permeability. **(b)** Relationship between content of carbonate cement and porosity/permeability. **(c)** Relationship between content of kaolinite and porosity/permeability. **(d)** Relationship between content of illite and porosity/permeability. **(e)** Relationship between content of chlorite and porosity/permeability.

role in enhancing the permeability of the reservoir (Li et al., 2024). Under the microscope, multiple phases of structural fractures can be observed (Figures 6H, 9P). They cut through debris particles, promoting late-stage dissolution modification and increasing porosity connectivity. In the 4,168.5–4,176 m interval of Well L 61, the rock is relatively dense, with an average porosity of 1.7% and a permeability of 0.3×10^{-3} μm^2. There are a total of 19 fractures, and at the fracture at 4,174.16 m, the permeability sharply increases to 5.1×10^{-3} μm^2. The permeability at the fractures was measured, with an average permeability of 3.45×10^{-3} μm^2 and a maximum of up to 53×10^{-3} μm^2. However, the correlation between porosity and permeability was not pronounced, indicating

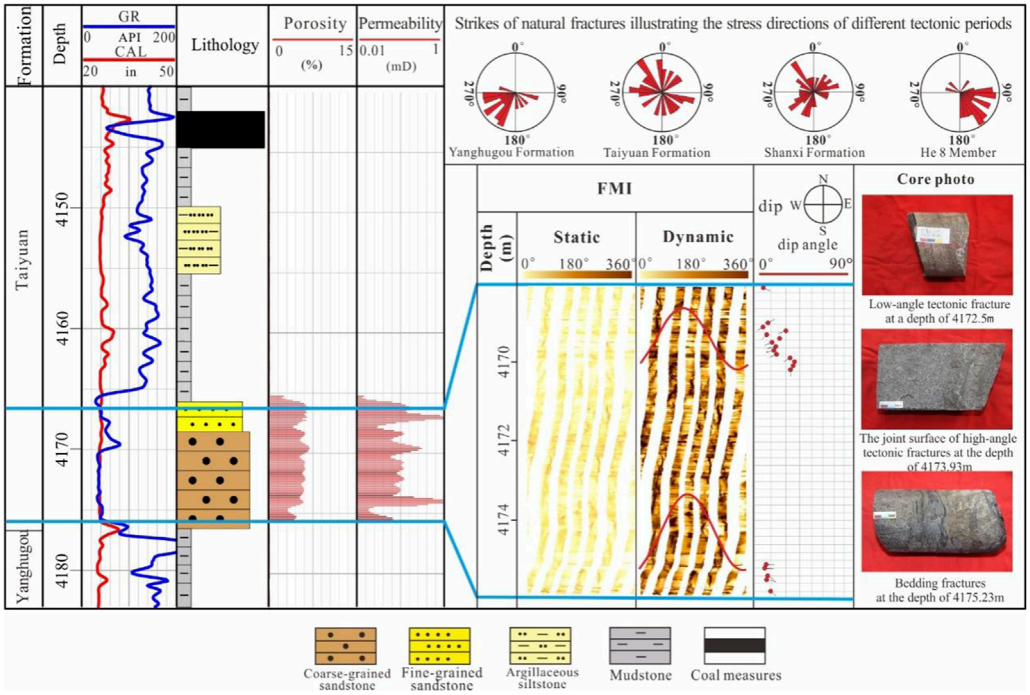

FIGURE 15
Imaging logging of fractures and reservoir physical properties.

that this controlling effect is limited and that it is essential to ensure that the original porosity of tight reservoirs is not compromised. If the original reservoir lacks sufficient resistance to compaction and has substantial pore filling, such fractures will not contribute significantly to the formation of high-quality reservoirs.

5.3 Formation mechanisms of reservoir rocks of different lithologies

Based on comprehensive analyses of reservoir characteristics, diagenesis, and primary controlling factors, we have elucidated the formation mechanisms of reservoir rocks across various lithologies.

Quartz sandstone reservoirs: Predominantly developed within the Yanghugou, Taiyuan, and Shihezi formations, these reservoirs are supplied by the Yinshan provenance. These reservoirs pore assemblages consisting of residual primary pores, lithic-dissolved pores, and intercrystalline pores. High-energy depositional environments, such as delta distributary channels, subaqueous distributary channels, tidal sand bars, and distributary channels, provide favorable conditions for the formation of high-quality reservoirs. The presence of magmatic rock fragments facilitates the development of particle-dissolved pores. With an average quartz content of approximately 81.36%, these rocks are capable of effectively preserving primary pores, while authigenic kaolinite infill further promotes the development of intercrystalline pores.

Lithic quartz sandstone reservoirs: These reservoirs are found across various formations and are influenced by multiple provenance supplies. Due to relatively strong compaction, the preservation of primary pores is adversely affected, leading to early densification. Microscopic examination reveals that grains are predominantly in line contact. However, long-term shallow-to-medium burial, combined with a high quartz content, inhibits compaction and protects intergranular pores. The pore assemblages in these reservoirs mainly comprise intergranular (dissolved) pores, lithic-dissolved pores, and intercrystalline pores. Depositional environments of rivers and deltas, particularly high-energy distributary channel sand bodies, mouth bars, tidal sand bars, and shallow lake sand bars, provide the material foundation for the formation of high-quality reservoirs. The high proportion of magmatic rock fragments favors the formation of lithic-dissolved pores, while the presence of pore-enhancing lithic particles and early-formed calcite cements helps preserve the integrity of primary pores. Early hydration of tuffaceous matrix locally alters to kaolinite, enhancing the compressive strength of sandstone and further promoting the development of intercrystalline pores.

Feldspathic sandstone reservoirs: Primarily developed in the Yanghugou and Taiyuan formations, these reservoirs are supplied by the Alashan provenance. The pore types in these reservoirs mainly include intergranular (dissolved) pores and feldspar-dissolved pores. Although the low content of detrital quartz does not provide significant protection to the intergranular volume, the relatively shallow burial diagenetic environment of the Alashan source-sink area results in weaker compaction, thereby favoring the preservation of primary pores. The high content of feldspar and magmatic rock fragments provides the necessary material conditions for the formation of particle-dissolved pores.

Lithic sandstone reservoirs: These reservoirs are mainly developed in the Shanxi and Shihezi formations, supplied by the North Qilian and North Qinling provenances. The primary storage

spaces are microfractures and intragranular dissolved pores. The depositional environment of the meandering river delta front during this period provided the material basis for reservoir formation. However, long-term deep burial has severely damaged intergranular pores. The high content of pore-reducing lithic fragments not only disrupts the pore structure between grains but also promotes the formation of quartz and other cements. Consequently, the high content of pore-reducing lithic fragments and muddy matrix results in the loss of primary pores after compaction, limiting the large-scale flow of acidic fluids and subsequent dissolution of the reservoir. As a result, the accompanying organic acids fail to extensively dissolve the reservoir, leading to the underdevelopment of secondary pores.

In summary, the formation mechanisms of reservoir rocks of different lithologies are influenced by a combination of depositional environments, provenance supplies, compaction, and diagenesis. These factors interact in complex ways to determine the pore assemblages and storage capacities of the resulting reservoirs.

6 Conclusion

The Upper Paleozoic reservoirs of the Ordos Basin are typically characterized by low to ultra-low porosity and low permeability tight sandstone reservoirs. They mainly consist of medium to coarse-grained quartz sandstone and lithic quartz sandstone. Diagenetic processes predominantly shaped the reservoir space, with dissolution pores being the primary type, supplemented by intergranular, intragranular, and fracture pores. When comparing the reservoir properties and micropore structures, the high-quality reservoirs were sequentially in the Taiyuan Formation, He 8 member, Yanghugou Formation, and Shanxi Formation.

Variations in depositional environments have led to differences in sand body thickness, rock granularity, mineral content, and structural features under different hydrodynamic conditions, ultimately governing reservoir quality. Within continental systems, fluvial channel margin/central reservoirs possess the highest quality, whereas natural levees have the lowest quality. In transitional marine–continental systems, distributary channels, subaqueous distributary channels, and barrier sandbank reservoirs are of the highest quality. Meanwhile, mouth bar and tidal channel reservoirs are of the lowest quality. The variability in the nature of the source rock in the provenance area causes differences in the composition of sandstone lithic fragments. This, in turn, leads to variability in the reservoir quality on a planar level.

Built upon sedimentation and provenance, diagenesis further dictates reservoir quality. The main diagenetic stages for the Upper Paleozoic reservoirs span from the syngenetic to mesogenetic B periods. They have divergent diagenetic evolutions and varying degrees of influence over the reservoir quality across these periods. During the early diagenetic stage, rapid burial and compaction were the primary drivers of the reservoir densification. Quartz grains resist compaction, preserving primary porosity. Meanwhile, early cementation by calcite occupies intergranular pores, preventing diagenetic fluids from dissolving and generating secondary pores, thus reducing the original porosity. In mesogenetic period A, dissolution contributed to the creation of substantial secondary porosity, whereas mesogenetic period B experienced a new wave of cementation, further diminishing the pore spaces. The impact of clay minerals on reservoir quality varies. Kaolinite plays a beneficial role, whereas illite filling intergranular spaces further densifies reservoirs. Fracture development is the primary contributor to the high permeability of reservoirs.

The main controlling factors of the formation of high quality tight sandstone are not single. The influences of local structure, sedimentary environment, provenance and diagenesis are considered in this paper. It is believed that with the deepening of research theories and research methods, more detailed research results will be revealed.

Data availability statement

The original contributions presented in the study are included in the article/supplementary material, further inquiries can be directed to the corresponding author.

Author contributions

CZ: Writing–original draft. SF: Writing–review and editing. JH: Writing–review and editing. LH: Writing–review and editing. AC: Writing–review and editing. YX: Writing–review and editing. HL: Writing–review and editing. YY: Writing–review and editing. HC: Writing–review and editing.

Funding

The author(s) declare that financial support was received for the research, authorship, and/or publication of this article. This work was supported by the National Natural Science Foundation of China (Nos 42202131 and 41872109); The “14th Five Year Plan” Prospective Basic Science and Technology Project, China National Petroleum Corporation (No. 2021DJ2101); and the Research Project of PetroChina Changqing Oilfield Company (No. CQYT-CQKTY-2021-JS-2728, 2020-62503).

Conflict of interest

Author JH was employed by Exploration and Development Research Institute of PetroChina Changqing Oilfield Company. Author LH was employed by SINOPEC Petroleum Exploration and Production Research Institute. Author YX was employed by SINOPEC Jianghan Oilfield Company.

The remaining authors declare that the research was conducted in the absence of any commercial or financial relationships that could be construed as a potential conflict of interest.

The authors declare that this study received funding from China National Petroleum Corporation. The funder had the following involvement in the study: study design and data collection.

Generative AI statement

The author(s) declare that no Generative AI was used in the creation of this manuscript.

Publisher's note

References

Aminul Islam, M. (2009). Diagenesis and reservoir quality of bhuban sandstones (neogene), titas gas field, bengal basin, Bangladesh. *J. Asian Earth Sci.* 35 (1), 89–100. doi:10.1016/j.jseaes.2009.01.006

Baker, J. C. (1991). Diagenesis and reservoir quality of the aldebaran sandstone, denison trough, east-central queensland, Australia. *Sedimentology* 38 (5), 819–838. doi:10.1111/j.1365-3091.1991.tb01874.x

Bao, H. P., He, D. F., Wang, Q. P., Zhang, L., Zhang, J. W., Yan, T., et al. (2022). Four main paleouplifts evolution in Ordos Basin and their differences in significance of oil and gas reservoir control. *J. Palaeogeogr.* 24 (05), 951–969. doi:10.7605/gdlxb.2022.05.068

Bloch, S., Lander, R. H., and Bonnell, L. (2002). Anomalously high porosity and permeability in deeply buried sandstone reservoirs: origin and predictability. *AAPG Bull.* 86 (2), 301–328. doi:10.1306/61EEDABC-173E-11D7-8645000102C1865D

Cao, Q., Gao, J. M., Fan, L. Y., Pang, C. X., and Yu, J. Z. (2015). Characteristics and significance of fluid inclusions in upper Paleozoic of southwest Ordos Basin. *Nat. Gas. Geosci.* 26 (12), 2245–2253. doi:10.11764/j.issn.1672-1926.2015.12.2245

Chen, L. H. (1990). *Application of scanning electron microscopy in petroleum geology*. Beijing: Petroleum Industry Press, 1–120.

Chen, S. Y., Hou, Z. S., and Zhang, S. (2015). Diagenesis characteristics of volcanic material in He 8 Member east block of Sulige Gas Field. *Fault-Block Oil Gas Field* 22 (02), 173–177.

Dai, J. X., Ni, Y. Y., and Wu, X. Q. (2012). Tight gas in China and its significance in exploration and exploitation. *Petroleum Explor. Dev.* 39 (3), 277–284. doi:10.1016/S1876-3804(12)60043-3

Darby, B. J., and Ritts, B. D. (2002). Mesozoic contractional deformation in the middle of the Asian tectonic collage: the intraplate Western Ordos fold-thrust belt, China. *Earth Planet. Sci. Lett.* 205 (1-2), 13–24. doi:10.1016/S0012-821X(02)01026-9

Dong, Y. X., Yang, S., Chen, L., Wang, Q., and Cao, Z. H. (2014). Braided river delta deposition and deep reservoirs in the Bohai Bay Basin: a case study of the Paleogene Sha 1 Member in the southern area of Nanpu Sag. *Petroleum Explor. Dev.* 41 (04), 429–436. doi:10.1016/S1876-3804(14)60049-5

Fan, J. M., Qu, X. F., Wang, C., Lei, Q. H., Cheng, L. B., and Yang, Z. Q. (2016). Natural fracture distribution and a new method predicting effective fractures in tight oil reservoirs in Ordos Basin, NW China. *Petroleum Explor. Dev.* 43 (5), 806–814. doi:10.1016/S1876-3804(16).30096-9

Fan, Q. M., Liu, X. F., Yao, J. L., Wang, Y. B., Wu, N., Xu, Q. H., et al. (2022). Characteristics of source rocks and Formation of reservoir bitumen in yinchuan graben, Ordos Basin, China. *Energies* 15 (13), 4809. doi:10.3390/en15134809

Gao, X. D., Wang, Y. B., Li, Y., Guo, H., Ni, X. M., Wu, X., et al. (2019). Characteristics of tight sandstone reservoirs and controls of reservoir quality: a case study of He 8 sandstones in the linxing area, eastern Ordos Basin, China. *Acta Geol. Sinica-English Ed.* 93, 637–659. doi:10.1111/1755-6724.13862

Geng, Y. S., Wang, X. S., Shen, Q. H., and Wu, C. M. (2007). Chronology of the precambrian metamorphic series in the Alxa area, inner Mongolia. *Geol. China* 34 (2), 251–261.

Guo, C. Q., Shen, Z. M., Zhang, L. Y., Xu, D. Q., Miao, D. Y., and Lu, X. C. (2003). The corrosion and its mechanism of organic acids on main minerals in oil-gas reservoir sand rocks. *Geology-Geochemistry* 31 (3), 53–57.

Han, C., Han, M., Jiang, Z. X., Han, Z. Z., Li, H., Song, Z. G., et al. (2019). Source analysis of quartz from the Upper Ordovician and Lower Silurian black shale and its effects on shale gas reservoir in the southern Sichuan Basin and its periphery, China. *Geol. J.* 54 (1), 438–449. doi:10.1002/gj.3192

Han, H. P., Wu, C. Y., Bai, Q. H., Chen, P., Liu, X. S., and Qin, B. P. (2014). Zircon U-Pb dating of clastic sandstone in the upper Paleozoic from Wushenqi area, Ordos Basin and its geological significance. *Acta Sedimentol. Sin.* 32 (4), 643–653. doi:10.14027/j.cnki.cjxb.2014.04.008

He, D. F., Sun, F. Y., Zhai, Y. H., Bao, H. P., Ma, J. H., and Kai, B. Z. (2021). Syncline development and tight sandstone gas accumulation model in Shigouyi area at western margin of Ordos Basin. *Oil and Gas Geol.* 42 (2), 370–390. doi:10.11743/ogg20210209

Hu, W. Q., Li, Y. B., Chen, X., Ma, L. T., Liu, C., Huang, Y., et al. (2020). Origin and source of natural gas in the upper paleozoic in linxing area, Ordos Basin. *Nat. Gas. Geosci.* 31 (1), 26–36. doi:10.11764/j.issn.1672-1926.2019.08.009

Kadkhodaie-Ilkhchi, R., Moussavi-Harami, R., Rezaee, R., Nabi-Bidhendi, M., and Kadkhodaie-Ilkhchi, A. (2014). Seismic inversion and attributes analysis for porosity evaluation of the tight gas sandstones of the Whicher Range field in the Perth Basin, Western Australia. *J. Nat. Gas Sci. Eng.* 21, 1073–1083. doi:10.1016/j.jngse.2014.10.027

Karim, A., Pe-Piper, G., and Piper, D. J. W. (2010). Controls on diagenesis of lower cretaceous reservoir sandstones in the western sable subbasin, offshore nova scotia. *Sediment. Geol.* 224 (1-4), 65–83. doi:10.1016/j.sedgeo.2009.12.010

Lee, E. Y., Novotny, J., and Wagreich, M. (2020). Compaction trend estimation and applications to sedimentary basin reconstruction (BasinVis 2.0). *Appl. Comput. Geosciences* 5, 100015. doi:10.1016/j.acags.2019.100015

Li, R. X., and Li, Y. Z. (2008). Tectonic evolution of the western margin of the Ordos Basin (Central China). *Russ. Geol. Geophys.* 49 (1), 23–27. doi:10.1016/j.rgg.2007.12.002

Li, Y. X., Zhang, H., and Tian, Y. F. (2015). Formation mechanism of coal source rocks and quartz overgrowths: an example of Shanxi formation in eastern Ordos Basin. *Bull. Geol. Sci. Technol.* 34 (6), 65–69.

Liu, R. E., Wu, H., Wei, X. S., Xiao, H. P., and Zhang, C. L. (2017). "Anomaly distribution and genesis of feldspar in the 8th Member sandstone reservoir of Shihezi formation. *Permian, Ordos Basin*. 46. 96–105.

Liu, S. B., Huang, S. J., Shen, Z. M., Lv, Z. X., and Song, R. C. (2014). Diagenetic fluid evolution and water-rock interaction model of carbonate cements in sandstone: an example from the reservoir sandstone of the Fourth Member of the Xujiahe Formation of the Xiaoquan-Fenggu area, Sichuan Province, China. *Sci. China Earth Sci.* 57 (5), 1077–1092. doi:10.1007/s11430-014-4851-2

Liu, X. S., Pan, X., Zhao, H. T., Wang, Z. L., Meng, P. L., Zheng, D. Y., et al. (2022). Control of differential diagenesis of tight sandstone reservoirs on the gas-water distribution: a case study on the Upper Paleozoic He 8 Member in the northern Tianhuan depression of the Ordos Basin. *Energy Explor. and Exploitation* 40 (1), 302–327. doi:10.1177/01445987211034590

Liu, Z. S., Liu, D. M., Cai, Y. D., Yao, Y. B., Pan, Z. J., and Zhou, Y. F. (2020). Application of nuclear magnetic resonance (NMR) in coalbed methane and shale reservoirs: a review. *Int. J. Coal Geol.* 218, 103261. doi:10.1016/j.coal.2019.103261

Lv, C. H., Huang, W. H., and Fei, L. (2017). The provenance analysis of the 8th member of the upper Paleozoic Shihezi formation in the western area of Ordos Basin. *Energy Sources, Part A Recovery, Util. Environ. Eff.* 39 (17), 1886–1893. doi:10.1080/15567036.2017.1381786

Oluwadebi, A. G., Taylor, K. G., and Dowey, P. J. (2018). Diagenetic controls on the reservoir quality of the tight gas collyhurst sandstone formation, lower permian, east Irish Sea Basin, United Kingdom. *Sediment. Geol.* 371, 55–74. doi:10.1016/j.sedgeo.2018.04.006

Pujol, M., Van Den Boorn, S., Bourdon, B., Brennwald, M., and Kipfer, R. (2018). Physical processes occurring in tight gas reservoirs from Western Canadian Sedimentary Basin: noble gas signature. *Chem. Geol.* 480, 128–138. doi:10.1016/j.chemgeo.2017.12.011

Qiu, L. W., Mu, X. J., Li, H., Zhang, J., Ge, J., Xu, S., et al. (2019). Characteristics of detritus development in the Permian lower Shihezi Formation in Hangjinqi area and its influence on reservoir physical properties. *Oil Gas Geol.* 40 (01), 24–33. doi:10.11743/ogg20190103

Shen, Z. H., Ruan, Z., Yu, B. S., Han, S. J., Bai, C. Y., Chang, Q. H., et al. (2022). Diagenetic fluid and its impact on sandstone reservoirs in the southern boxing sag, dongying depression. *Bohai Bay Basin, China* 2022, 25. doi:10.1155/2022/4981422

Song, K. P., Luo, J. L., Liu, X. S., Hou, Y. D., Sheng, W. Y., Cao, J. J., et al. (2020). Characteristics and genetic mechanism of carbonate cements in Upper Paleozoic tight sandstones, southwestern Ordos Basin. *Nat. Gas. Geosci.* 31 (11), 1562–1573.

Stroker, T. M., Harris, N. B., Crawford Elliott, W., and Marion Wampler, J. (2013). Diagenesis of a tight gas sand reservoir: upper cretaceous mesaverde group, piceance basin, Colorado. *Mar. Petroleum Geol.* 40, 48–68. doi:10.1016/j.marpetgeo.2012.08.003

Su, N. N., Song, F., Qiu, L. W., and Zhang, W. (2021). Diagenetic evolution and densification mechanism of the upper paleozoic tight sandstones in the Ordos Basin, northern China. *J. Asian Earth Sci.* 205, 104613. doi:10.1016/j.jseaes.2020.104613

Sun, N. L., Zhong, J. H., Liu, S. G., Tian, D. E., Liu, C., Cao, M. C., et al. (2017). Diagenesis and physical property evolution of gravity flow tight reservoir of Yanchang formation in southern Ordos Basin. *Earth Sci.* 42, 1802–1816.

Taylor, T. R., Giles, M. R., Hathon, L. A., Diggs, T. N., Braunsdorf, N. R., Birbiglia, G. V., et al. (2010). Sandstone diagenesis and reservoir quality prediction: models, myths, and reality. *AAPG Bull.* 94 (8), 1093–1132. doi:10.1306/04211009123

Tian, J. C., Wu, Q., Wang, F. N., Lin, X., Zhang, J. Q., and Cao, T. S. (2011). Research on development factors and the deposition model of large area reservoir sandstones of He8 section of Xiashihezi Formation of Permian in Ordos Basin. *Acta Petrol. Sin.* 27 (8), 2403–2412.

Tian, J. F., Gao, Y. L., Zhang, P. B., Yu, J., and Zhang, Z. G. (2022). Genesis and geological implication of illite coatings of triassic yanchang Formation in Ordos Basin. *Lithol. Reserv.* 34 (2), 54–65.

Wang, J. W., Bao, Z. D., Chen, M. J., Sun, F. J., Liu, R. E., Zhao, M. F., et al. (2005). Differentiation of sandstones' tuff fillings and its effect on porosity - an example from the Paleozoic sandstones in Northwestern Ordos. *Sci. Geol. Sin.* 03, 429–438.

Wang, Y. Z. (2017). *Provenance and sedimentary characteristics of Shan-1 and the He 8 Member in the middle part of Tianhuan depression*. Beijing: China University of Geosciences.

Wang, Z. T., Zhou, H. R., Wang, X. L., Zheng, M. P., Santosh, M., Jing, X. C., et al. (2016). Detrital zircon fingerprints link western north China craton with east gondwana during ordovician. *Gondwana Res.* 40, 58–76. doi:10.1016/j.gr.2016.08.007

Weedman, S. D., Brantley, S. L., and Albrecht, W. (1992). Secondary compaction after secondary porosity: can it form a pressure seal? *Geology*, 20(4), 303–306. doi:10.1130/0091-7613(1992)020<0303:scaspc>2.3.co;2

Wei, H. (2002). *Research on Permian-Carboniferous depositional systems and the sequence stratigraphy of Ordos area*. (dissertation/doctoral thesis). Northwest University, China (Xi'an).

Wei, W., Azmy, K., and Zhu, X. M. (2022). Impact of diagenesis on reservoir quality of the lacustrine mixed carbonate-siliciclastic-volcaniclastic rocks in China, 233.105265

Wei, X. S., Xiao, H. P., Liu, R. E., Kang, R., Nan, J. X., and Hao, A. S. (2017). Pickling effect of the abnormal heat and its relation to disappearance of feldspar of the upper Paleozoic in the Ordos Basin. *Acta Geosci. Sin.* 91 (09), 2139–2149.

Wu, H. H., Liu, R. E., Zuo, Z. F., and Wang, H. C. (2020). Gas and water distribution characteristics and its main controlling factors of the Upper Paleozoic tight sandstone reservoirs in the northern Tianhuan depression. *J. China Univ. Min. Technol.* 49 (01), 148–158.

Xia, Y. P., Xu, L. G., Zhen, L. H., Liu, W. H., and Lv, Y. S. (2005). Structural features and oil-gas prospecting targets of thrusting fault belt in western edge of Ordos Basin. *Pet. Geol.* 10 (5), 13–19.

Xiao, D. S., Lu, S. F., Yang, J. X., Zhang, L. C., and Li, B. (2017). Classifying multiscale pores and investigating their relationship with porosity and permeability in tight sandstone gas reservoirs. *Energy fuels.* 31 (9), 9188–9200. doi:10.1021/acs.energyfuels.7b01487

Xiao, H. P., Liu, R. E., Zhang, F. D., Lin, C. S., and Zhang, M. Y. (2019). Sedimentary model reconstruction and exploration significance of permian He 8 member in Ordos Basin, NW China. *Petroleum Explor. Dev.* 46 (2), 280–292. doi:10.1016/S1876-3804(19)60008-X

Yang, H., Fu, J. H., Liu, X. S., and Meng, P. L. (2012). Accumulation conditions and exploration and development of tight gas in the Upper Paleozoic of the Ordos Basin. *Petroleum Explor. Dev.* 39 (3), 315–324. doi:10.1016/S1876-3804(12)60047-0

Yang, H., Fu, S. T., and Wei, X. S. (2004). Geology and exploration of oil and gas in the Ordos Basin. *Appl. Geophys* 1 (2), 103–109. doi:10.1007/s11770-004-0011-3

Yang, R. C., Fan, A. P., Van Loon, A. J., Han, Z. Z., and Wang, X. P. (2014). Depositional and diagenetic controls on sandstone reservoirs with low porosity and low permeability in the eastern sulige gas field, China. *Acta Geol. Sin. Engl. Ed.* 88 (5), 1513–1534. doi:10.1111/1755-6724.12315

Yang, Z., He, S., Guo, X. W., Li, Q. Y., Chen, Z. Y., and Zhao, Y. C. (2016). Formation of low permeability reservoirs and gas accumulation process in the daniudi gas field, northeast Ordos Basin, China. *Mar. Petroleum Geol.* 70, 222–236. doi:10.1016/j.marpetgeo.2015.10.021

Yang, Z., and Zou, C. N. (2022). Orderly "symbiotic enrichment" of conventional and unconventional oil and gas: discussion on theory and technology of conventional and unconventional petroleum geology. *Acta Geol. Sin.* 96 (5), 1635–1653.

Zhang, F. D., Li, J., Wei, G. Q., Liu, X. S., Guo, J. Y., Li, J., et al. (2018). Formation mechanism of tight sandstone gas in areas of low hydrocarbon generation intensity: a case study of the Upper Paleozoic in North Tianhuan Depression in Ordos Basin, NW China. *Petroleum Explor. Dev.* 45 (1), 79–87. doi:10.1016/s1876-3804(18)30007-7

Zhang, L. Q., Zhang, H. F., Zhang, S. S., Xiong, Z. L., Luo, B. J., Yang, H., et al. (2017). Lithospheric delamination in post-collisional setting: evidence from intrusive magmatism from the North Qilian orogen to southern margin of the Alxa block, NW China. *Lithos* 288-289, 20–34. doi:10.1016/j.lithos.2017.07.009

Zhang, Y. Y., Jiang, S., He, Z. L., Wang, Y. B., Guo, M. Q., Zhu, G. H., et al. (2022). Characteristics of heterogeneous diagenesis and modification to physical properties of Upper Paleozoic tight gas reservoir in eastern Ordos Basin. *J. Petroleum Sci. Eng.* 208, 109243. doi:10.1016/j.petrol.2021.109243

Zhao, P. K., and Ji, Y. L. (2005). Sedimentary facies on the upper Paleozoic of the oreland basin of the western margin of the Ordos. *Xinjiang Geol.* (02), 152–157+216.

Zhao, W. T., Hou, G. T., and Hari, K. R. (2016). Two episodes of structural fractures and their stress field modeling in the Ordos Block, northern China. *J. Geodyn.* 97, 7–21. doi:10.1016/j.jog.2016.02.005

Zheng, Q. H., and Liu, Y. Q. (2015). Microscopic pore structure and movable fluid saturation of ultra low permeability reservoir. *Bull. Geol. Sci. Technol.* 34 (4), 124–131.

Zhou, A. C., Jia, B. W., Ma, M. L., and Zhang, H. (2001). The whole sequences of volcanic event deposits on the north margin of the North China plate and their features. *Geol. Rev.* 47, 175–183.

Zhou, J. S., Qiao, X. Y., Wang, R. G., Yin, X., Cao, J., Cao, B. F., et al. (2022). Effective reservoir development model of tight sandstone gas in Shanxi Formation of Yan'an gas field, Ordos Basin. *Nat. Gas. Geosci.* 33 (2), 195–206. doi:10.11764/j.issn.1672-1926.2021.08.007

Zhou, X. F., Zhao, L. X., and Jiao, S. J., (2016). Features of illite films in tight sandstone reservoir of Ordos Basin. *J. Xi'an Shiyou Univ. Nat. Sci. Ed.*, 31(6), 1–8.

Zhu, P., Meng, X. H., Wang, X., Dong, Y. X., Li, X. W., Zhang, C. H., et al. (2022). Geochemical characteristics of diagenetic fluid and densification model of tight gas sandstone reservoirs in Linxing area, eastern margin of Ordos Basin, China. *China* 138, 105496. doi:10.1016/j.marpetgeo.2021.105496

Zou, C. N. (2014). *Unconventional petroleum geology*. Beijing: Geological Publishing House, 1–145.

Zou, C. N., Yang, Z., Zhang, G. S., Tao, S. Z., Zhu, R. K., Yuan, X. J., et al. (2019). Establishment and practice of unconventional oil and gas geology. *Acta Geol. Sin.* 93 (1), 12–23.